Engineering Structures 157 (2018) 300–315

Contents lists available at ScienceDirect

Engineering Structures

journal homepage: www.elsevier.com/locate/engstruct

# A mechanical model for failures in shear of members without transverse reinforcement based on development of a critical shear crack

Francesco Cavagnis*, Miguel Fernández Ruiz, Aurelio Muttoni

*École Polytechnique Fédérale de Lausanne, ENAC, Station 18, CH-1015 Lausanne, Switzerland*

ARTICLE INFO

*Keywords:*
Concrete structures
Shear strength
Critical shear crack theory
Shear-transfer actions

ABSTRACT

In this paper, a mechanical model consistent with the main assumptions of the Critical Shear Crack Theory (CSCT) is proposed for shear design of slender concrete members without shear reinforcement. To that aim, the shear force that can be transferred through the critical shear crack by aggregate interlock, residual tensile strength and dowelling action as well as due to the inclination of the compression chord are calculated by integration of fundamental constitutive laws accounting for the critical shear crack opening and kinematics at failure. The pertinence of the assumptions is validated through comparisons to detailed test measurements to assess their validity. The model allows predicting the failure load, the deformation capacity and the location of the critical shear crack leading to failure. The results are checked against large datasets and the model is finally used to discuss on the influence of the various parameters on the governing shear-transfer actions. The results are eventually used to propose improvements on the CSCT failure criterion for shear, relating the shear strength and its associated deformation capacity.

## 1. Introduction

The shear strength of reinforced concrete beams without transverse reinforcement has been extensively investigated in the past and many mechanical approaches have been proposed to address this issue [1–7]. Yet, these models present significant discrepancies on the mechanical parameters and shear-transfer actions governing failure and this is still a topic of controversy and open discussion. As established since long, there are various potential shear-carrying actions that allow transferring shear forces in cracked concrete members. They are usually classified as beam shear-transfer actions (where the force in tension chord varies)—cantilever action (Fig. 1a), residual tensile strength of concrete (Fig. 1b), dowelling action (Fig. 1c) aggregate interlock (Fig. 1d), which may also be combined (Fig. 1e)—and the arching action (where the force in the tension tie remains constant, Fig. 1f). A complete description of each of them can be found elsewhere [8].

One mechanical approach which considers the contribution of all potential shear-carrying actions is the Critical Shear Crack Theory (CSCT) proposed by Muttoni et al. [3]. This theory is based on the assumption that the shear strength of slender members without stirrups is governed by the development of a critical shear crack that limits the strength of the theoretical inclined compression strut carrying shear. According to this theory, both the shear strength and the deformation capacity of a member are related through a failure criterion (Fig. 1g), with lower strengths associated to larger deformation capacities (and thus larger crack widths).

A detailed description of the CSCT and of the development of the critical shear crack can be found elsewhere [8–11]. These investigations have shown that rather different crack patterns may develop for similar reinforced concrete members and that the contribution of each-shear transfer action may significantly vary during loading (being this strongly dependent on the shape, location and kinematics of the critical shear crack).

A theoretical description of the main physical parameters governing the shear capacity can be found in Fernández Ruiz et al. [8]. This work shows, by means of an analytical approach based on simple constitutive laws, that all shear-transfer actions depend eventually on the same mechanical parameters (concrete compressive strength, effective depth, maximum aggregate size and crack width). These results confirmed the validity of the failure criterion of the CSCT relating the shear strength and the deformation capacity at failure (Fig. 1g) in terms of its shape and governing parameters. Since that work [8], a number of detailed testing programmes using digital image correlation (DIC) have been performed [10–12]. These programmes provide very detailed information on the development of the critical shear crack and on the associated capacity of each shear-transfer action. In this paper, this new experimental data is used in combination with refined constitutive laws to perform detailed calculations on the contribution of the various

* Corresponding author.
*E-mail address:* francesco.cavagnis@epfl.ch (F. Cavagnis).

https://doi.org/10.1016/j.engstruct.2017.12.004
Received 28 February 2017; Received in revised form 20 October 2017; Accepted 4 December 2017

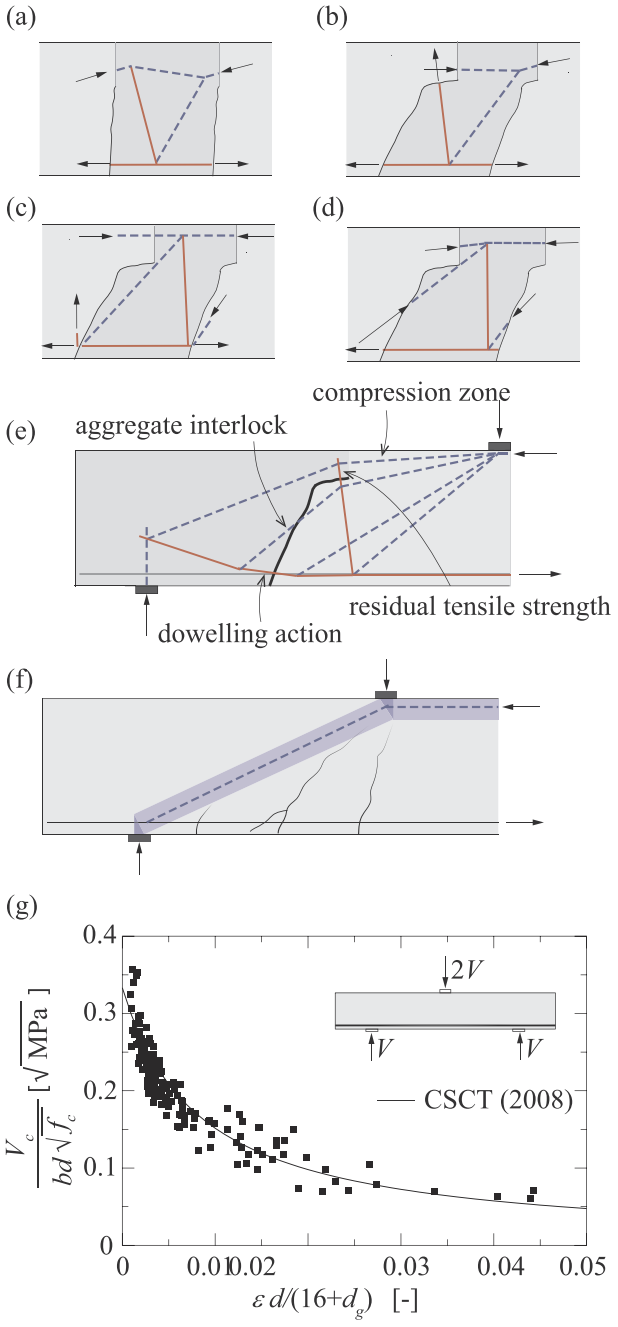


**Fig. 1.** Shear-transfer actions described with strut and tie models (tensile forces in red and compressive forces in blue): (a) cantilever action; (b) residual tensile strength of concrete; (c) dowelling action; (d) aggregate interlock; (e) combined shear-transfer actions; (f) arching action; (g) failure criterion of the Critical Shear Crack Theory (CSCT) (adapted from Muttoni et al. [3]). (For interpretation of the references to colour in this figure legend, the reader is referred to the web version of this article.)

potential shear-transfer actions during the process of loading and at failure. As a result, predictions can be made not only on the strength and deformation capacity, but also on the shape and location of the critical shear crack as well as on the amount of the shear carried by each shear-transfer action. The results are compared to actual tests to show the consistency of the approach and to discuss on the role and significance of the various shear-transfer actions. On that basis, improvements on the CSCT failure criterion will be presented and discussed.

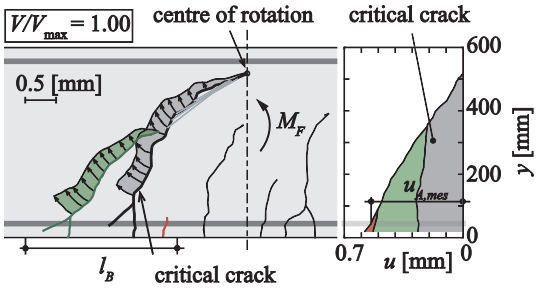


**Fig. 2.** Crack kinematics, centre of rotation and horizontal opening $u$ of the cracks tributory to the opening of the critical shear crack in a region of length $l_B$ (specimen SC69 [11]).

## 2. Load-critical shear crack opening relationship

One of the main assumptions of the CSCT, according to Muttoni et al. [3], is that the opening $w$ of the critical shear crack can be assumed to be proportional to the product of the longitudinal strain in a control section times the effective depth of the member ($w \propto \varepsilon \cdot d$, where the strain $\varepsilon$ can be calculated according to a cracked sectional analysis). The validity of this assumption has been confirmed by recent experimental investigations [11] on the basis of DIC measurements. According to these measurements, although cracks at narrow spacing may develop at the level of the longitudinal reinforcement, they merge thereafter and the sum of all cracks tributary to the critical shear crack yields an approximately linear profile of the horizontal component of the crack width (refer to Fig. 2). This tributary length $l_B$ has been experimentally observed to be fairly constant at peak load [11] and can be approximated by the expression:

$$l_B = d - c \tag{1}$$

(average of measured-to-calculated values equal to 1.01 with a Coefficient of Variation of 7% for 11 specimens presented in [11]), where $c$ is the depth of the compression zone, calculated by assuming a linear response of concrete in compression and neglecting concrete in tension:

$$c = d \cdot \rho \cdot \frac{E_s}{E_c}\left(\sqrt{1 + \frac{2 \cdot E_c}{\rho \cdot E_s}} - 1\right) \tag{2}$$

with $E_c$ taken as $E_c = 10'000 f_c^{1/3}$ in MPa.

Thus, considering that the reinforcement strains can be calculated as (linear profile of compression stresses):

$$\varepsilon_s = \frac{M_F}{A_s \cdot E_s \cdot z} = \frac{M_F}{A_s \cdot E_s \cdot (d - c/3)} \tag{3}$$

and assuming that the horizontal crack opening at the level of the reinforcement is proportional to the product of the tributary length $l_B$ times the strain at the level of the longitudinal reinforcement ($u_A = \varepsilon_s \cdot l_B$), it results:

$$u_A = \frac{M_F}{A_s \cdot E_s} \cdot \frac{d - c}{d - c/3} \tag{4}$$

In simply supported elements subjected to point load, for instance, $M_F = V_F \cdot a_F$ and thus Eq. (4) yields:

$$u_A = \frac{V_F \cdot a_F}{A_s \cdot E_s} \cdot \frac{d - c}{d - c/3} \tag{5}$$

where $a_F$ refers the moment-to-shear ratio of the investigated section, corresponding to the distance $x_F$ of the section to the support in this case (the so called shear span, see Fig. 3a).

It has to be noted that Eq. (3) is an approximation as the contribution of the internal forces acting on the critical shear crack (refer to Fig. 3d) to the moment $M_F$ at a section located at crack tip are neglected

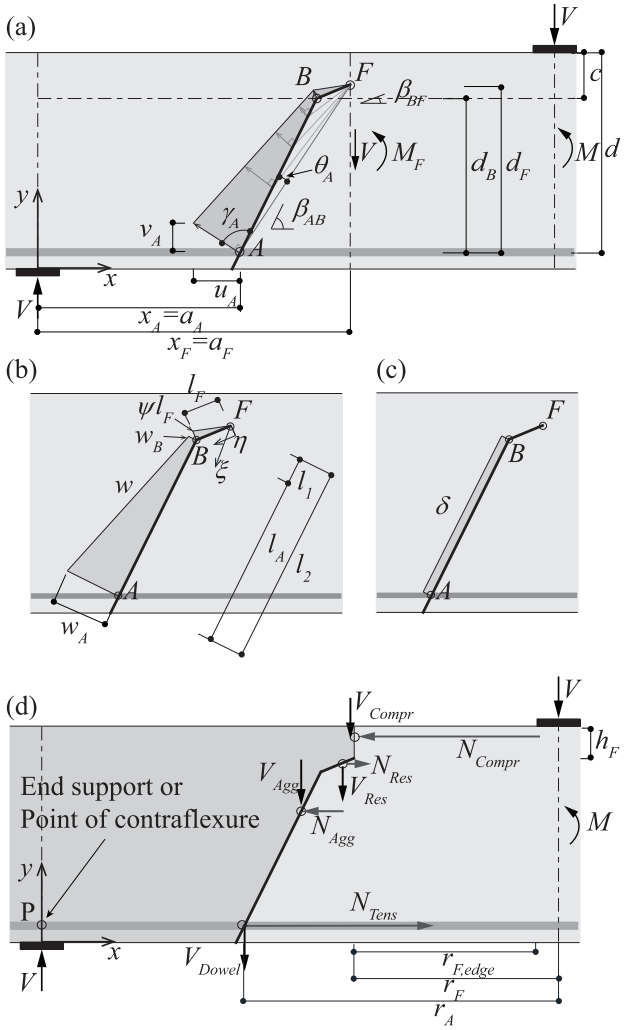


**Fig. 3.** (a) Kinematics and displacements of the crack lips according to the adopted crack shape; (b) crack opening $w$ perpendicular to the crack surface and (c) sliding $\delta$; (d) equilibrium of the rigid-body and internal forces.

(in accordance to the numerical results of detailed calculations accounting for all potential forces in the critical shear crack [11]).

## 3. Contribution of the shear-transfer actions

In the following, the contribution of the various shear-transfer actions to the shear resistance will be investigated by integration of fundamental constitutive laws. This will be done with reference to a potential critical shear crack characterized by a given shape and kinematics (crack opening and sliding). The location of the potential critical shear crack will then be varied in order to find the governing location leading to the minimum shear strength.

### 3.1. Crack shape and kinematics

The shape of the critical shear crack for slender members failing in shear has been investigated in detail and described by Cavagnis et al. [10]. The critical crack at failure can be approximated by a bi-linear shape comprising a quasi-vertical part (segment A-B in Fig. 3a, whose inclination is related to the moment-to-shear ratio [10]) and a quasi-horizontal part (segment B-F in Fig. 3a), geometry also assumed by other researchers [4,6,13,14].

A trend for the inclination of the quasi-vertical segment A-B with respect to the moment-to-shear ratio $\alpha_A$ was experimentally investigated in [11] and approximated by the following expression:

$$\beta_{AB} = \frac{\pi}{4}\cdot\left(1 + \frac{\alpha_A^{1/3}}{3}\right) \tag{6}$$

where $\alpha_A$ is the shear slenderness ratio defined as $\alpha_A = \frac{M_A}{V_A \cdot d}$, with $M_A$ and $V_A$ corresponding to the acting bending moment and shear at the section where the investigated crack intercepts the flexural reinforcement (section $x_A$).

The length $l_A$ of the segment A-B of the crack can be calculated assuming that it propagates up to the neutral axis [10]:

$$l_A = \frac{d-c}{\sin\beta_{AB}} \tag{7}$$

With respect to the quasi-horizontal part of the crack, it was observed that its origin is related to the (quasi-vertical) tensile stresses developing at the tip of the crack, due to the cantilever action between the flexural cracks (Kani's tooth model, Fig. 1a, [3,11]) and that it propagates at a load level which can be significantly lower than the failure load. Although the length $l_F$ and the angle $\beta_{BF}$ of the segment B-F were observed to have some level of scatter [3], in the following, $l_F$ is assumed in a simplified manner to be equal to $d/6$ and $\beta_{BF}$ equal to $\pi/8$ in agreement to experimental measurements [10,11].

The kinematics of such crack is presented in Fig. 3b and c. According to [8] and to the measurements of [11], it can be assumed that the centre of rotation is approximately located at the tip of the crack. The rotation of the crack can thus be calculated as a function of the reinforcement strain:

$$\psi = \frac{u_A}{d_F} = \frac{\varepsilon_s \cdot l_B}{d_F} \tag{8}$$

where $u_A$ and $\varepsilon_s$ are respectively the horizontal opening of the crack and the strain at the level of the longitudinal reinforcement, $l_B$ is the length contributing to the opening of the critical crack according to Eq. (1) (see Fig. 2) and $d_F = d - c + l_F \cdot \sin\beta_{BF}$ defines the distance from the tip of the crack to the flexural reinforcement (Fig. 3b and c). The associated relative movements are depicted in Fig. 3a. The shape and kinematics allow defining the opening and sliding at each point of the critical crack (opening in Fig. 3b and sliding in Fig. 3c). It can be noted that the top part of the crack is characterized by pure opening (mode I), whereas the quasi-vertical part by a combined crack opening and sliding (mixed mode I-II).

### 3.2. Residual tensile strength contribution

Cracked concrete has a residual capacity to transfer tensile stresses for low crack openings. The softening behaviour can be modelled using several approaches. In this work, the proposal by Reinhardt [15] characterized by a simple power law equation will be used:

$$\sigma_{res} = f_{ct} \cdot \left(1 - \left(\frac{w}{w_c}\right)^{c_1}\right) \geqslant 0 \tag{9}$$

where $c_1 = 0.31$ and $w_c = G_F/f_{ct} \cdot (1 + c_1)/c_1$ represents the maximum crack width for stress transfer. The fracture energy of ordinary normal weight concrete $G_F$ can be calculated according to *fib* Model Code 2010 [16] as $G_F = 0.073 \cdot f_c^{0.18}$ (N/mm,MPa) and the tensile strength of concrete is assumed equal to $f_{ct} = 0.3 \cdot f_c^{2/3}$ for $f_c < 50$ MPa [16] and $f_{ct} = 0.3 \cdot (50 \cdot f_c)^{1/3}$ for $f_c \geq 50$ MPa (approximating [16]). It shall be noted that the *fib* Model Code 2010 does not explicitly account for the size of the aggregates on the value of the fracture energy. Nevertheless, this dependence is acknowledged by the code in its commentary and also considered in previous versions of the *fib* Model Code (as that of 1990 [17]), implying that the shear transfer capacity of the residual tensile strength depends eventually upon the aggregate size [8].

It is important to note that only the top part of the critical shear crack (segment B-F) is characterized by a response in mode I and it is

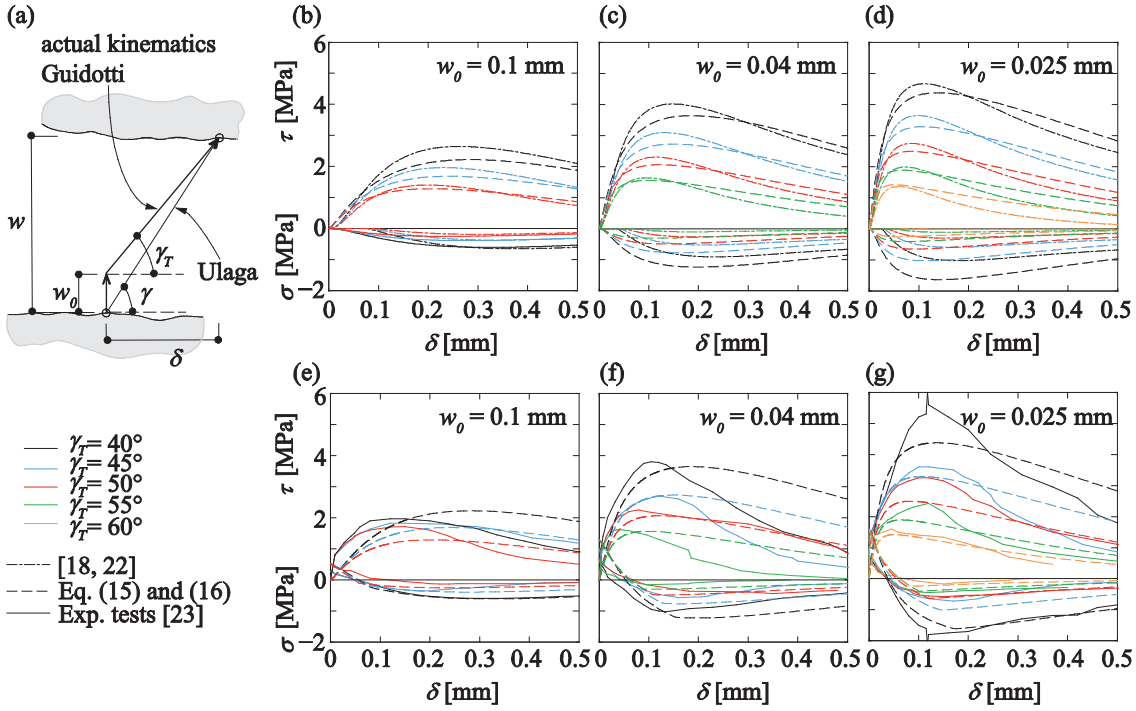


**Fig. 4.** (a) Kinematics of mixed mode tests performed by Jacobsen et al. ($f_c$ = 41 MPa, $d_g$ = 8 mm) [23]; (b–d) comparisons of aggregate interlock stresses according to the model of Walraven [18] for kinematics analogue to that of Guidotti [22] and the aggregate interlock stresses calculated according to Eqs. (15) and (16) but neglecting the term $\sigma_{res}$; (e–g) comparison of mixed mode test results [23] with shear and normal stresses calculated according to Eqs. (15) and (16).

then governed by residual tensile strength of concrete. The quasi-vertical part (segment A-B) is characterized by a mixed mode response so that the residual concrete tensile strength in that part is considered together with the aggregate interlock contribution (see following subsection). By integration of the stresses along segment B-F, the shear force can be determined as:

$$V_{Res} = \int_0^{l_{F1}} \sigma_{res} \cdot b \cdot \cos\beta_{BF} \cdot d\eta \tag{10}$$

where $\eta$ is the integration variable, $l_{F1}$ is the integration limit, $b$ is the width of the member, $\sigma_{res}$ refers to the residual stress normal to the crack and $\beta_{BF}$ to the angle of segment B-F.

The resulting shear force carried by the residual tensile strength of concrete according to Eq. (10) thus results:

$$V_{Res} = f_{ct} \cdot b \cdot \cos\beta_{BF} \int_0^{l_{F1}} \left(1 - \left(\frac{\psi \cdot \eta}{w_c}\right)^{c_1}\right) \cdot d\eta = f_{ct} \cdot b \cdot \cos\beta_{BF} \cdot l_{F1} \cdot \left(1 - \frac{1}{1 + c_1} \cdot \left(\frac{u_A \cdot l_{F1}}{d_F \cdot w_c}\right)^{c_1}\right) \tag{11}$$

and the associated normal force is:

$$N_{Res} = V_{Res} \cdot \tan\beta_{BF} \tag{12}$$

The integration of stresses leads to two possible regimes: (i) cases where the normal stresses develop along the whole length of segment B-F ($\psi \cdot l_F \leqslant w_c$) so that $l_{F1} = l_F$ and (ii) cases where the normal stresses develop only close to the tip of the crack ($\psi \cdot l_F > w_c$), with $l_{F1}$ equal to:

$$l_{F1} = \frac{w_c}{\psi \cdot l_F} \cdot l_F = \frac{w_c}{u_A} \cdot d_F \tag{13}$$

It is interesting to note that for the latter case, Eqs. (11) and (13) give a simple expression:

$$V_{Res} = \frac{G_F \cdot b \cdot \cos\beta_{BF} \cdot d_F}{u_A} \tag{14}$$

where the residual strength contribution depends on the fracture energy of concrete $G_F$ and not on the distribution of the tensile stresses (Eq. (9)). In addition, Eq. (14) clearly shows the hyperbolic decay of the contribution $V_{Res}$ with increasing crack opening $u_A$ (in agreement to [8]).

### 3.3. Aggregate interlock contribution

Many approaches based on the opening and sliding between the rough surfaces of the crack have been proposed in the literature to calculate the aggregate interlock stresses [18–20]. A consistent approach to this issue was developed by Walraven [18], as a two-phase model, whose application has been generalized by Ulaga [21] and Guidotti [22] accounting for different kinematical paths. A detail description of them can be found in [9,22]. However, the integration of Walraven's equations requires numerical procedures and it cannot be solved in a closed-form manner. In order to avoid the use of numerical procedures in this work, two analytical equations have been calibrated by the authors of this paper on the basis of the Walraven's model for aggregate interlock, but considering the kinematics of Guidotti which is more representative of the actual case (see Fig. 2). These assumptions allow calculating the transferred shear stresses ($\tau$) for a given opening ($w$) and sliding ($\delta$) as:

$$\tau_{agg} = \tau_{agg,0} = \sqrt{f_c} \cdot \frac{c_3 \cdot \overline{\delta}^{4/3}}{(c_2 \overline{w})^{1.8 + c_2 \cdot \overline{\delta}}} \tag{15}$$

as well as the normal stresses ($\sigma$):

$$\sigma_{agg} = \sigma_{res} - \sigma_{agg,0} = \sigma_{res} - \sqrt{f_c} \cdot \frac{c_4 \cdot \overline{\delta}^{7/3}}{(c_2 \overline{w})^{3 + c_2 \cdot \overline{\delta}}} \tag{16}$$

where $\sigma_{res}$ is defined according to Eq. (9), $c_2$ = 40, $c_3$ = 35 and $c_4$ = 400 are constants; $\overline{\delta} = \delta / d_{dg}$ and $\overline{w} = w / d_{dg}$ are the normalized crack sliding and crack opening and $d_{dg}$ is an average roughness whose value can be calculated as follows:

$$\begin{aligned} d_{dg} &= \min(40\text{ mm}, 16 + d_g) && \text{for } fc \leqslant 60\text{ MPa} \\ d_{dg} &= \min(40\text{ mm}, 16 + d_g \cdot (60/f_c)^2) && \text{for } f_c > 60\text{ MPa} \end{aligned} \tag{17}$$

where $d_g$ refers to the maximum aggregate size. Justification of Eq. (17) is provided later in this section.

Fig. 4b–d shows comparisons between the aggregate interlock stresses according to the model of Walraven [18] for a kinematics analogue to that of Guidotti [22] (initial opening $w_0$ followed by a combined opening and sliding, Fig. 4a) and the normal and shear stresses calculated according to Eqs. (15) and (16), but neglecting the term $\sigma_{res}$ which is not accounted for in the theoretical model of Walraven. The same comparisons are shown in Fig. 4e–g to aggregate interlock stresses measured by Jacobsen et al. [23] for specimens tested with the same kinematics, but accounting for the term $\sigma_{res}$ (which is actually present in the tests). It can be noted that the peak value of the calculated shear and normal stresses is in good agreement with the theoretical and experimental ones, as well as the stiffness and softening properties. In addition, the simple superposition of the residual tensile stresses ($\sigma_{res}$) and aggregate interlock stresses ($\sigma_{agg,0}$) gives reasonable results compared to the test measurements (Fig. 4e–g): it can be observed that the normal stresses vary from tension to compression during the combined opening $w$ and sliding $\delta$, but remain in tension for low values of $\delta$.

It is important to mention that Eqs. (15) and (16) have been calibrated to be applied to calculate the aggregate interlock stresses for mixed mode crack openings, with initial openings $w_0$ and secant mixed mode angle $\gamma$ (variable along the quasi-vertical segment of the crack, according to the kinematics of Fig. 3b and c) which are typical for critical shear cracks of slender members ($\gamma > 45°$, [10]). With respect to the average roughness ($d_{dg}$), this term accounts for two issues:

- The first is that concrete cracks, present an undulated (rough) surface (Fig. 5b and d), contrary to Walraven's approach which assumes cracks as perfect planar surfaces with protruding aggregates (Fig. 5a and c). This roughness, ensuring the transfer of shear forces by interlocking, is referred to as meso-roughness [8]. The value of the meso-roughness depends on the surface properties after crack development, but can be assumed as 16 mm [3] for normal cases (refer to Eq. (17)).
- The second is that, as observed by Sherwood et al. [24], the increase of the interlock capacity is limited for large aggregates. In addition, for high-strength concrete ($f_c > 60$ MPa), a reduction of the aggregate size shall be considered [3], since cracks develop through the aggregates, resulting in crack surfaces that are relatively smooth [25].

As shown in Fig. 3a, only the quasi-vertical branch of the critical shear crack (segment A-B) is characterized by a mixed mode I and II behaviour. On the basis of the aggregate interlock laws and the relative displacements between the lips of the crack, the aggregate interlock forces at the critical crack can be determined as:

$$V_{Agg} = b\cdot\left(\int_{l_1}^{l_2}\tau_{agg,0}\cdot\sin\beta_{AB}\,d\xi - \int_{l_1}^{l_2}\sigma_{agg,0}\cdot\cos\beta_{AB}\,d\xi\right) + b\cdot\int_{l_1}^{l_3}\sigma_{res}\cdot\cos\beta_{AB}\,d\xi = V_{Agg,0} + V_{Agg,res} \tag{18}$$

$$N_{Agg} = b\cdot\left(\int_{l_1}^{l_2}\tau_{agg,0}\cdot\cos\beta_{AB}\,d\xi + \int_{l_1}^{l_2}\sigma_{agg,0}\cdot\sin\beta_{AB}\,d\xi\right) - b\cdot\int_{l_1}^{l_3}\sigma_{res}\cdot\sin\beta_{AB}\,d\xi = N_{Agg,0} + N_{Agg,res} \tag{19}$$

where $\xi$ is the integration variable, $l_1$, $l_2$ and $l_3$ are the integration limit, $b$ is the width of the member, $\tau_{agg,0}$, $\sigma_{agg,0}$ and $\sigma_{res}$ are defined in Eqs. (15) and (16) and $\beta_{AB}$ refers to the inclination of segment A-B. Note that the integration of $\tau_{agg,0}$ and $\sigma_{agg,0}$ leads to $V_{Agg,0}$ and $N_{Agg,0}$, whereas the integration of $\sigma_{res}$ leads to $V_{Agg,res}$ and $N_{Agg,res}$.

In a general manner, the resulting shear force that can be transferred by aggregate interlock can be written as7:

$$\begin{aligned}\frac{V_{Agg}}{\sqrt{f_c}\cdot b} &= \int_{l_1}^{l_2}\frac{\sin\beta_{AB}\cdot c_3\cdot\overline{\delta_A}^{4/3}}{\left(c_2\cdot\psi\cdot\frac{\xi}{d_{dg}}\right)^{1.8+c_2\cdot\overline{\delta_A}}} - \frac{\cos\beta_{AB}\cdot c_4\cdot\overline{\delta_A}^{7/3}}{\left(c_2\cdot\psi\cdot\frac{\xi}{d_{dg}}\right)^{3+c_2\cdot\overline{\delta_A}}}d\xi \\ &\quad + \int_{l_1}^{l_3}\cos\beta_{AB}\cdot\left(1-\left(\frac{\psi\cdot\xi}{w_c}\right)^{c_1}\right)d\xi \\ &= \sin\beta_{AB}\cdot\frac{c_3\cdot\overline{\delta_A}^{4/3}}{(c_2\overline{\delta_A}+0.8)\cdot\left(\frac{u_A}{d_F}\cdot\frac{c_2}{d_{dg}}\right)^{1.8+c_2\overline{\delta_A}}}\cdot\frac{l_2^{0.8+c_2\overline{\delta_A}}-l_1^{0.8+c_2\overline{\delta_A}}}{(l_2\cdot l_1)^{0.8+c_2\overline{\delta_A}}} \\ &\quad -\cos\beta_{AB}\cdot\frac{c_4\cdot\overline{\delta_A}^{7/3}}{(c_2\overline{\delta_A}+2)\cdot\left(\frac{u_A}{d_F}\cdot\frac{c_2}{d_{dg}}\right)^{3+c_2\overline{\delta_A}}}\cdot\frac{l_2^{2+c_2\overline{\delta_A}}-l_1^{2+c_2\overline{\delta_A}}}{(l_2\cdot l_1)^{2+c_2\overline{\delta_A}}} \\ &\quad +\cos\beta_{AB}\cdot\left[l_3\cdot\left(1-\frac{1}{1+c_1}\cdot\left(\frac{u_A\cdot l_3}{d_F\cdot w_c}\right)^{c_1}\right)-l_1\cdot\left(1-\frac{1}{1+c_1}\cdot\left(\frac{u_A\cdot l_1}{d_F\cdot w_c}\right)^{c_1}\right)\right]\cdot \\ &\quad \frac{f_{ct}}{\sqrt{f_c}}\end{aligned} \tag{20}$$

where $\overline{\delta_A} = \frac{\delta_A}{d_{dg}} = \frac{\sqrt{u_A^2+v_A^2}\cdot\sin\theta_A}{d_{dg}}$, $v_A = \frac{u_A}{d_F}\cdot(l_F\cdot\cos\beta_{BF} + l_A\cdot\cos\beta_{AB})$ and $\theta_A = \beta_{AB} - \text{atan}\frac{d_F}{l_F\cdot\cos\beta_{BF}+l_A\cdot\cos\beta_{AB}}$ (refer to Fig. 3a).

The integration limits $l_1$ and $l_2$ can be calculated on the basis of the geometry of the crack (refer to Fig. 3a): $l_1 = l_F\cdot\cos(\beta_{AB}-\beta_{BF})$ and $l_2 = l_1 + l_A$. With respect to $l_3$, the integration of aggregate interlock stresses leads to three potential regimes:

(i) cases where the residual stresses $\sigma_{res}$ develop through the whole length of segment A-B ($w_A < w_c$ corresponding to low crack openings), hence $l_3$ is equal to $l_2$; (ii) cases where the residual stresses develop only on the top region of the segment A-B ($w_B < w_c < w_A$) so that $l_3$ results:

$$l_3 = \frac{w_c}{w_A}\cdot l_2 \tag{21}$$

and (iii) cases where no residual tensile stresses develop through the quasi-vertical branch of the crack since the opening of the crack along the whole segment A-B exceeds $w_c$ (corresponding to large crack openings), hence $l_3$ is equal to $l_1$ and $V_{Agg,res}$ and $N_{Agg,res}$ are equal to zero.

### 3.4. Dowelling action

Dowelling forces can be activated due to relative vertical displacement between the crack surfaces at the level of the longitudinal reinforcement [9]. The capacity of dowelling action to transfer shear is governed by the effective area of the concrete in tension near the bars and by its effective tensile strength [26]:

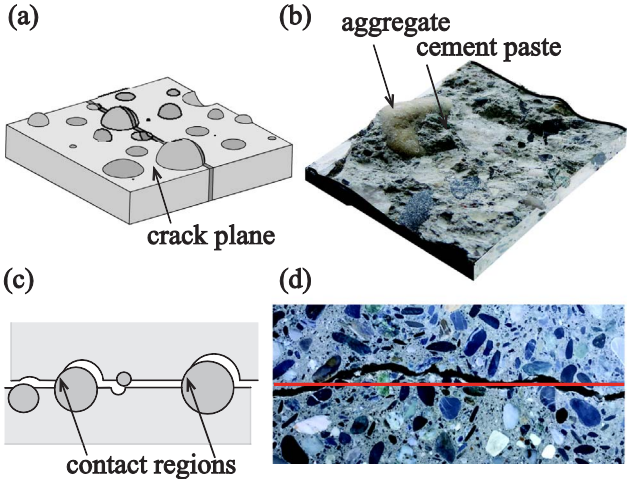


**Fig. 5.** (a) Idealized crack plane according to the model of Walraven [18] and (b) actual crack plane; crack surface near the aggregates: (c) idealized, according to the Walraven [18] and (d) actual.

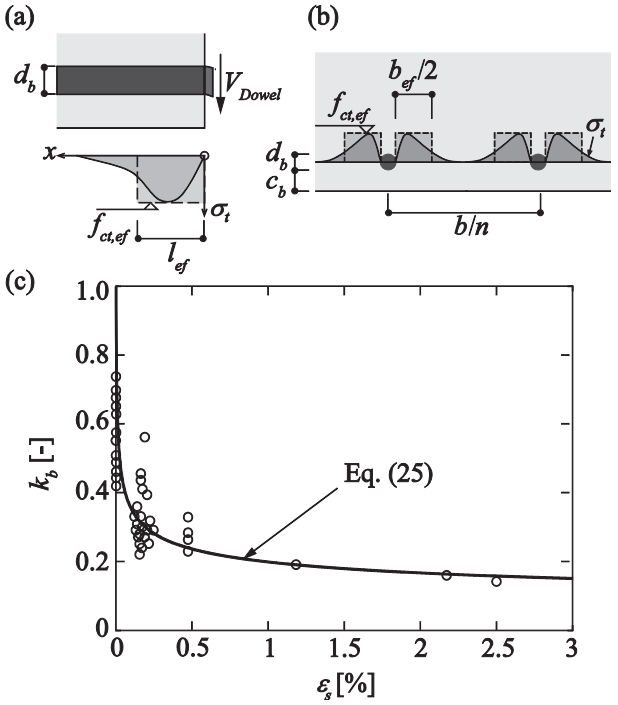


**Fig. 6.** (a) Development of transverse stresses at the cover region along the bar and definition of effective length $l_{ef}$; (b) distribution of transverse tensile stresses (perpendicular to the bar) and definition of effective width $b_{ef}$ (adapted from [26]); (c) reduction of the effective tensile strength as a function of the longitudinal strains in the bar (experimental data from [27]).

$$V_{Dowel} = n \cdot f_{ct,ef} \cdot b_{ef} \cdot l_{ef} \tag{22}$$

where $n$ is the number of bars activated, $f_{ct,ef}$ is the effective tensile strength, $b_{ef}$ and $l_{ef}$ are the effective width and length in which the tensile strength develops (Fig. 6a and b). The effective length is estimated as $l_{ef} = 2d_b$ [26] (where $d_b$ is the diameter of the reinforcing bars, Fig. 6a) and the effective width $b_{ef}$ (Fig. 6b) can be calculated as [26]:

$$b_{ef} = \min[b/n - d_b, 4 \cdot c_b] \tag{23}$$

where $b$ is the width of the member and $c_b$ is the concrete cover.

With respect to the effective tensile strength of concrete ($f_{ct,ef}$), it should be noted that its value is strongly influenced by the state of strains in the flexural reinforcement (due to its interaction with bond [26]). This effect can be estimated as [27]:

$$f_{ct,ef} = k_b \cdot f_{ct} \tag{24}$$

where $k_b$ is a strength reduction factor and it follows a decay for increasing strains in the flexural reinforcement (Fig. 6c). When the reinforcement is not strained, $k_b$ can be assumed equal to 1. In the following, the reduction factor for increasing value of strains in the longitudinal reinforcement is calibrated by fitting the experimental data presented in [27] as (refer to Fig. 6c):

$$k_b = 0.063 \cdot \varepsilon_s^{-1/4} \leqslant 1 \tag{25}$$

By replacing the steel strain $\varepsilon_s$ with the value $\varepsilon_s = u_A/l_B$, the coefficient $k_b$ becomes:

$$k_b = 0.063 \cdot \left(\frac{l_B}{u_A}\right)^{1/4} = 0.063 \cdot \left(\frac{d-c}{u_A}\right)^{1/4} \leqslant 1 \tag{26}$$

The shear resistance due to dowelling action of one-ways slabs with one layer of reinforcement bars is thus:

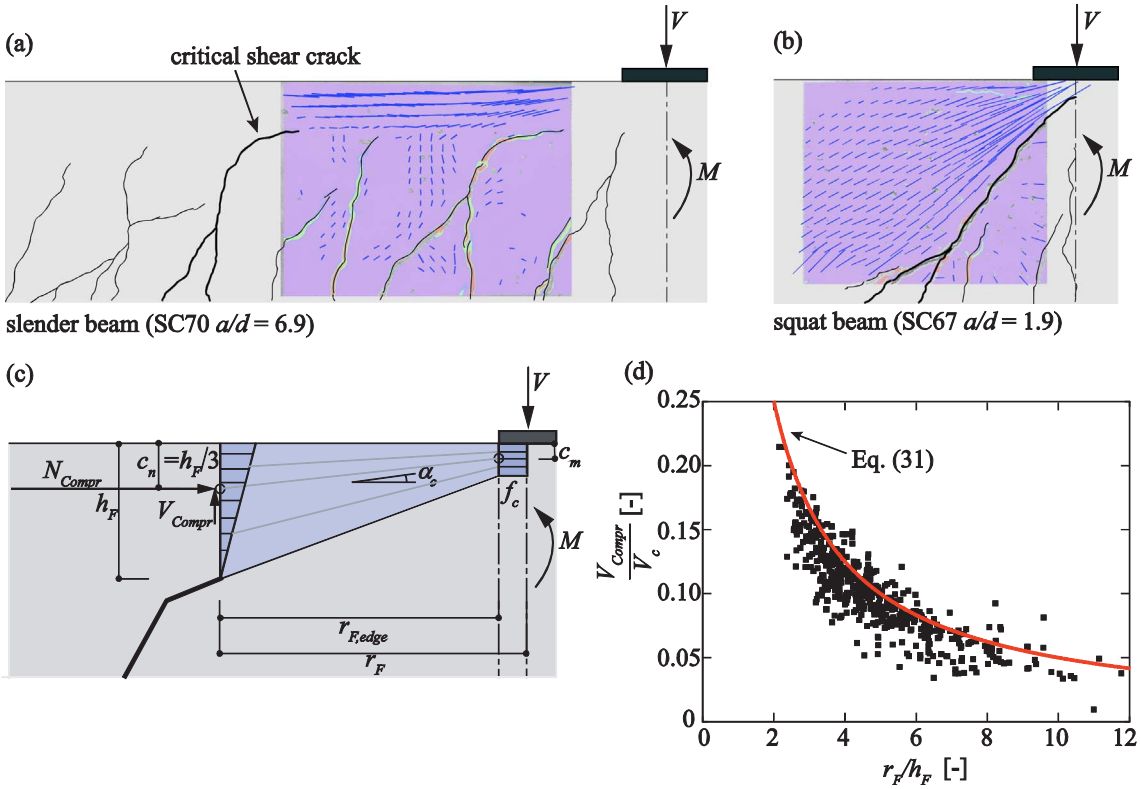


**Fig. 7.** Crack pattern and principal compressive strains at failure load for (a) a slender beam (specimen SC70) and (b) a squat beam (specimen SC67) (adapted from Cavagnis et al. [11]); (c) hyphothesis of a stress field used to determine the contribution to the shear strength of the compression zone; (d) calculated contribution of the compression zone with respect to the calculated shear capacity as a function of the distance between the tip of the crack and the axis where the load is applied (tests included in the database by Reineck et al. [31], assuming $x_A = 0.5a$).

$$V_{Dowel} = k_b \cdot f_{ct} \cdot n \cdot (b/n - d_b) \cdot 2 \cdot d_b \quad (27)$$

For comparison with test data, when no information is available on the bar spacing or for multiple layers, a value of $3d_b$ will be assumed as bar spacing. With this assumption, the last part of Eq. (27) becomes $4n \cdot d_b^2$ which can be expressed as a function of the reinforcement ratio ($16\rho \cdot b \cdot d/\pi$) so that the shear strength due to the dowel contribution can be approximated by:

$$V_{Dowel} \approx 5 \cdot k_b \cdot f_{ct} \cdot \rho \cdot b \cdot d \quad (28)$$

### 3.5. Contribution of the compression zone

Shear can also be transferred by means of the inclination of the compression chord [8]. For slender beams, this action is significant mostly before the propagation of the segment B-F of the critical crack within the compression zone and then it decreases progressively as the inclination of the compression chord is rather flat (Figs. 1e and 7a) [11]. For short-span beams (associated to low slenderness), with cracks developing without disturbing the theoretical direct strut (typically cracks whose tip is located close to the acting load), the arching action can develop almost undisturbed and the shear strength is mostly controlled by this action (refer to Figs. 1f and 7b).

A realistic assumption for the inclination of the compression zone is derived based on the detailed observations of the principal strain directions shown in Fig. 7a and b and in [11] (assuming that the inclination of principal strains and stresses is parallel). According to these measurements, it can be assumed that the resultant of the forces of the compression zone at the section corresponding to point F acts at a distance $c_n = 1/3\ h_F$ from the top compressive fibre, where $h_F$ is the thickness of the compression zone above the tip of the crack ($h_F = d - d_F$). In addition, at the edge of the loading plate, a stress block of thickness $2\,c_m$ with compressive stresses equal to the full compressive strength $f_c$ can be assumed (refer to Fig. 7c). This can be presumed to be a lower-bound of the actual contribution, as the tensile stresses perpendicular to the strut are neglected. The horizontal and vertical component acting in the compression zone can thus be calculated iteratively by moment equilibrium of the rigid body with respect to point of contraflexure (point P in Fig. 3d). The iterative procedure involves assuming an initial distance $c_m$ between the top compressive fibre and the centre of the theoretical strut at the edge of the loading plate, which allows defining the inclination $\alpha_c$ of the compression zone:

$$\tan\alpha_c = \frac{c_n - c_m}{r_{F,edge}} \quad (29)$$

where $r_{F,edge}$ is the distance between the tip of the crack and the edge of the loading plate (Fig. 7c).

Varying the value of $c_m$, the iterative procedure ends when $\sigma$ reaches the compressive strength of concrete $f_c$ and the vertical component results:

$$V_{Compr} = N_{Compr} \cdot \frac{c_n - c_m}{r_{F,edge}} = f_c \cdot b \cdot 2 \cdot c_m \cdot \frac{c_n - c_m}{r_{F,edge}} \quad (30)$$

Since the location of the critical shear crack is unknown, the iterative procedure that allows calculating the contribution of the compression zone shall be performed for any potential shear crack in the span of the member. It can be noted that an increase of the moment-to-shear ratio of the critical shear crack leads to an increase of the normal force in the compression zone and thus to an increase also of the contribution of the compression chord [7]. In Fig. 7d, the contribution of the compression zone is calculated for 629 slender beams included in the database by Reineck et al. [31], assuming $x_A = 0.5a$ for all tests. It can be observed that the percentage of the total shear carried by the compression zone depends significantly on the ratio $r_F/h_F$, where $r_F$ is the distance between the tip of the crack and the axis where the load is applied. As the contribution of the compression zone shown in Fig. 7d is relatively low for slender beams compared to other shear-transfer actions, a simplified expression can be used despite the non-negligible scatter:

$$\frac{V_{Compr}}{V_c} = \frac{k_c \cdot h_F}{r_F} < 1 \quad (31)$$

where $V_c$ is the total shear capacity ($V_c = V_{Res} + V_{Agg} + V_{Dowel} + V_{Compr}$) and $k_c$ is a constant obtained by fitting of the calculated contribution of the compression zone and that can be assumed equal to 0.5. It is important to mention that when a direct strut can develop, this approach is no longer valid since the theoretical strut carries almost the total shear force (refer to Fig. 7b). This is for instance the case of members with low shear-to-span ratios ($a/d < 2.5$), with high pre-stressing forces (associated to low effective slenderness [28]), or with no or limited bond strength [3].

The shear carried by the inclination of the compression chord yields thus from Eq. (31):

$$V_{Compr} = \frac{k_c \cdot h_F/r_F}{1 - k_c \cdot h_F/r_F} \cdot (V_{Res} + V_{Agg} + V_{Dowel}) \quad (32)$$

It can be noted that according to this approach, the contribution of the compression zone is determined by the geometry and the location of the critical shear crack and it is governed by the same mechanical parameters as the other shear-transfer actions.

## 4. Evaluation of the shear capacity

The total shear strength $V_c$ can be calculated by summing the contribution of the various shear-transfer actions:

$$V_c = V_{Res} + V_{Agg} + V_{Dowel} + V_{Compr} = \frac{V_{Res} + V_{Agg} + V_{Dowel}}{1 - k_c \cdot h_F/r_F} \quad (33)$$

The three components $V_{Res}$, $V_{Agg}$ and $V_{Dowel}$ contained in Eq. (33) are strain-dependent, which means that they can be expressed as a function of the crack opening $u_A$ (see Eqs. (11), (20) and (22)). The crack opening $u_A$ can be calculated using Eq. (4) which means that an iteration is required (as the crack opening depends on the shear force $V$). Calculating the shear strength requires thus assuming a location of the critical crack and then iteratively increasing the crack opening and checking that the acting shear force $V$ is equal to the shear capacity $V_c$. The solution $V = V_c$ is the intersection between the load-deformation relationship of Eq. (4) and the failure criterion of Eq. (33) as shown in Fig. 8a. The governing location of the critical shear crack can therefore be calculated as the one leading to the minimum strength of all potential locations.

The iterative procedure for calculation of the strength can be summarized in the following steps:

(1) Choose a location of the critical shear crack $x_A$.
(2) Calculate the angle $\beta_{AB}$ as a function of $\alpha_A = M_A/(V_A \cdot d)$ according to Eq. (6) (refer to Fig. 3a).
(3) Assume an initial crack opening $u_{Ai}$ (as a first step $u_{A0} = 0.001$ mm can be assumed).
(4) Calculate, as a function of the shape of the crack and its kinematics, the residual tensile strength force ($V_{Res}$, Eq. (11) in Section 3.2), the aggregate interlock force ($V_{Agg}$, Eq. (20) in Section 3.3), the dowelling action ($V_{Dowel}$, Eq. (22) in Section 3.4), the contribution of the compression zone ($V_{Compr}$, Eq. (32) in Section 3.5) and the shear capacity as the sum of these contributions ($V_c$, Eq. (33)).
(5) Calculate the crack opening $u_A$ as a function of the acting bending moment at the section corresponding to the tip of the crack ($M_F$), (refer to Eq. (4) in Section 2), where $M_F$ is proportional to the shear force ($V$).
(6) Iterate the crack opening $u_{Ai}$ at step 3 and repeat from step 3 to 6, until $u_A$ is equal to $u_{Ai}$.

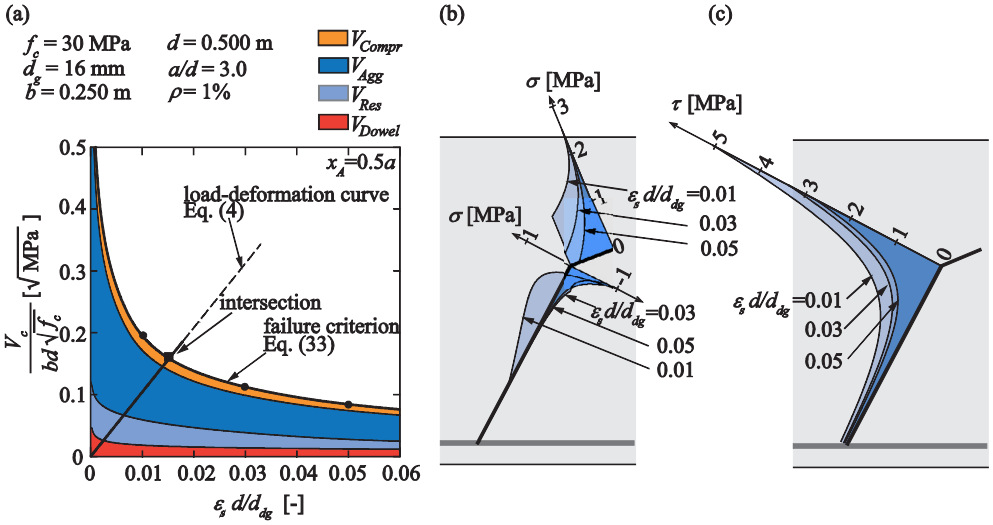


**Fig. 8.** (a) Failure criterion and load-deformation curve; shear-transfer actions: aggregate interlock, residual tensile strength of concrete, dowelling action and contribution of the compression zone; (b) normal and (c) shear stresses developing along the critical shear crack for three different values of $\varepsilon_s d/d_{dg}$ (0.01, 0.03 and 0.05).

One of the main advantages of this approach is that it can be applied to general or more complex cases and to different loading conditions. This can be done by accounting for the influence of the main governing mechanical parameters (moment-to-shear ratio $a_F$, crack opening, reinforcement ratio, aggregate size, compressive strength) and evaluating the contribution of the different load-carrying actions at the peak load.

Fig. 8a shows an instance of the contribution of the different shear-transfer actions to the shear strength as a function of the strains at the level of the longitudinal reinforcement. The example refers to a simply supported beam without transverse reinforcement subjected to point loading. The failure criterion in Fig. 8a is expressed as a function of the parameter $\varepsilon_s \cdot d/d_{dg}$, where the product $\varepsilon_s \cdot d$ is assumed to be proportional to the crack opening. Such normalization is consistent to that used by the CSCT [3] (Fig. 1g) and allows for a direct comparison. It can be observed that in this example the aggregate interlock is the governing shear-transfer action and that the contribution of the concrete in tension is significant for low openings of the critical shear crack. On the contrary, the contribution of the compression zone and the longitudinal bars (dowelling action) to the shear strength are very limited in this case. Moreover, it can be noted that the strength of each shear-transfer action decreases for increasing opening of the critical crack and that their decay follows a similar trend (in agreement to [8]). The reason for this strength decay with increasing crack opening $u_A$ is illustrated in Fig. 8b and c, where the residual tensile stresses ($\sigma_{res}$) and the aggregate interlock stresses ($\sigma_{agg}$ and $\tau_{agg}$) are shown for three different values of the opening of the shear crack ($\varepsilon_s \cdot d/d_{dg}$ = 0.01, 0.03 and 0.05). It can be noted that the normal stress $\sigma_{agg}$ is in tension in a part of segment A-B for low openings of the critical shear crack ($\varepsilon_s \cdot d/d_{dg}$ = 0.01), whereas for larger openings it is always in compression (consistently to experimental observations of other researchers [23,29]). With respect to the shear stress $\tau_{agg}$, it reaches a maximum value of 5 MPa in the upper part of the segment A-B and it decreases for increasing openings of the critical shear crack.

## 5. Discussion on the significance of shear-transfer actions and their dependence on the critical shear crack development for members subjected to point load

In Fig. 9 the location of the critical crack and the associated capacities of the shear-transfer actions are investigated with reference to an actual test (specimen SC61, presented in detail in [10]). The specimen corresponds to a simply supported beam tested under concentrated load ($a/d$ = 4.41, $d$ = 556 mm, $\rho$ = 0.89%, $f_c$ = 35.3 MPa, $d_g$ = 16 mm). Three different potential positions of the critical shear crack ($x_A = d$, $x_A = 0.5a$ and $x_A = a - d$) are investigated. Their inclinations $\beta_{AB}$ are calculated according to Eq. (6) and correspond well with the observed cracks (Fig. 9a). From Fig. 9b–d it can be noted that the strains at the level of the longitudinal reinforcement and the contribution of the different shear-transfer actions vary as a function of the location of the critical shear crack. It can be observed that the contribution of aggregate interlock is dominant in this case for all investigated positions of the critical shear crack. Moreover, when the crack is located close to support (in a general case, the point of contraflexure with zero bending moment), the contribution of the compression zone is very limited and the tensile strength of concrete plays a role, whereas when the critical crack develops closer to the load introduction plate (section of maximum bending moment), the contribution of the compression zone increases and the shear carried by the tensile strength of concrete decreases. In a general manner, the governing theoretical position of the critical crack is defined as the location where the sum of the contributions of the different shear-transfer actions reaches its minimum value. In Fig. 9b–d, it can be observed that the shear capacity (sum of all shear-transfer actions) does not significantly vary between the investigated sections $x_A$ and that the location of the critical crack has thus a limited influence on the shear strength of the member. This explains why for this type of members, the experimentally observed position of the failure crack can present a large scatter and different shear-transfer actions may eventually be governing [8,11].

The governing location of the critical crack is also investigated in Fig. 10 for different values of slenderness ratio ($a/d$), reinforcement ratio ($\rho$) and effective depth ($d$). In Fig. 10a, the contribution of the different shear-transfer actions to the shear capacity is shown for each position $x_A$ of the critical shear crack. It can be observed that for cracks developing within a region between 0.4$a$ and 0.6$a$, the total shear capacity is almost constant but the amount of shear carried by each shear-transfer actions shows some level of variation. In Fig. 10b and c it can be observed that an increase of the slenderness ratio leads to a variation of the governing position of the critical crack, with the governing crack closer to mid-span for less slender members. In Fig. 10d it can be noted that the distance $r_F$ between the tip of the critical shear crack and the axis where the load is applied varies between $d$ and 2$d$. A similar trend, concerning the location of the governing critical shear crack has been experimentally observed in the tests performed by Leonhardt and Walther [30]. The influence of the reinforcement ratio is also illustrated in Fig. 10e. An increase in the reinforcement ratio leads to an increase of the height of the compression zone, which therefore plays a more significant contribution in carrying the shear. Consequently, for increasing values of the reinforcement ratio, the governing location of the critical crack shifts towards mid-span. It can be shown that almost all other parameters have low influence on the governing position of the

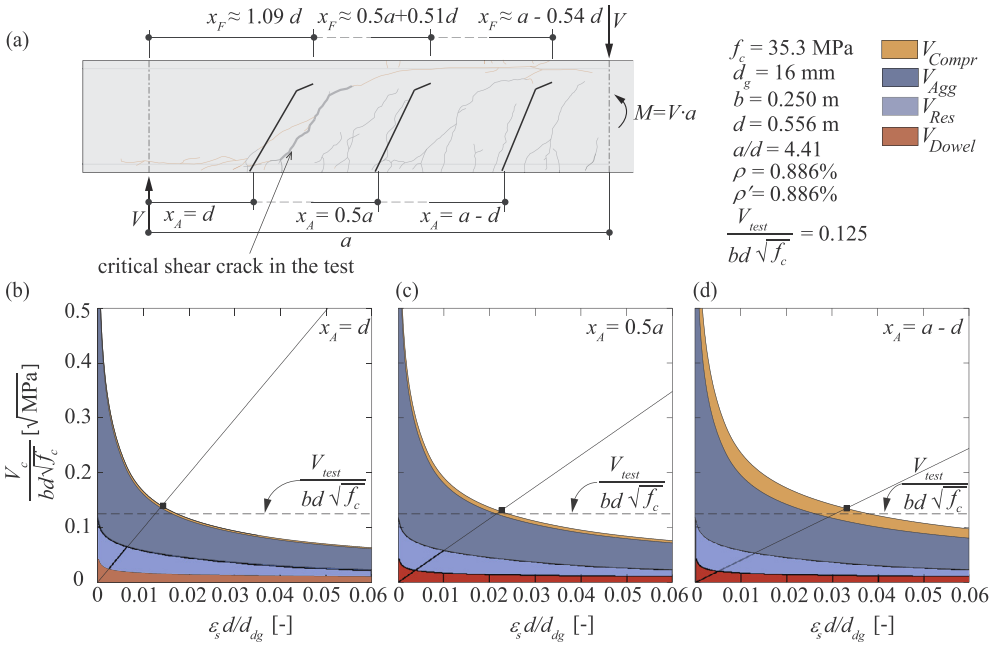


**Fig. 9.** (a) Specimen SC61 [10]: crack pattern (cracks in black for increasing load until maximum load, cracks in red after failure) and selected potential locations of the critical shear crack $x_A$; (b–c–d) contribution of the various shear-transfer actions at the different locations of the critical shear crack ($x_A = d$, $x_A = 0.5a$ and $x_A = a - d$), intersection of the load-deformation relationship with the failure criterion and comparison with the experimental result.

critical shear crack (Fig. 10f).

An interesting fact to be noted is that the curves representing the shear capacity are very flat around the minimum (at a distance $r_A$ between $1.5d$ and $2.25d$ from the load introduction plate and at a value of $x_A$ between $0.4a$ and $0.6a$). For these cases, adopting a fixed control section within this region is even sufficient for calculating the shear strength (although the relative significance of the shear-transfer actions may not be accurately assessed). To that aim, for instance, a value $x_A = 0.5a$ in agreement with the considerations of Reineck et al. [31] is reasonable.

In Fig. 11, the calculated shear capacity of 635 rectangular concrete beams without shear reinforcement (data from Reineck et al. [31] completed with the tests by Cavagnis et al. [11]) is plotted against the normalized crack width parameters. The plot is normalized to account for the effective depth, the width, the compressive strength and the aggregate size of the member [8]. The black points in Fig. 11 represent the intersection between the failure criteria calculated according to Eq. (33) at the control section $x_A = 0.5a$ and the load-deformation relationship (refer to Eq. (5)). In addition, the direction of the failure envelopes in the vicinity of the intersection is plotted (grey lines in Fig. 11). It is interesting to note that failures occur actually in a narrow band despite the large range of cases considered (effective depth $d$ ranging 50–2000 mm, flexural reinforcement ratio ρ ranging 0.4–7%, concrete strength $f_c$ ranging 10–110 MPa, aggregate size $d_g$ ranging

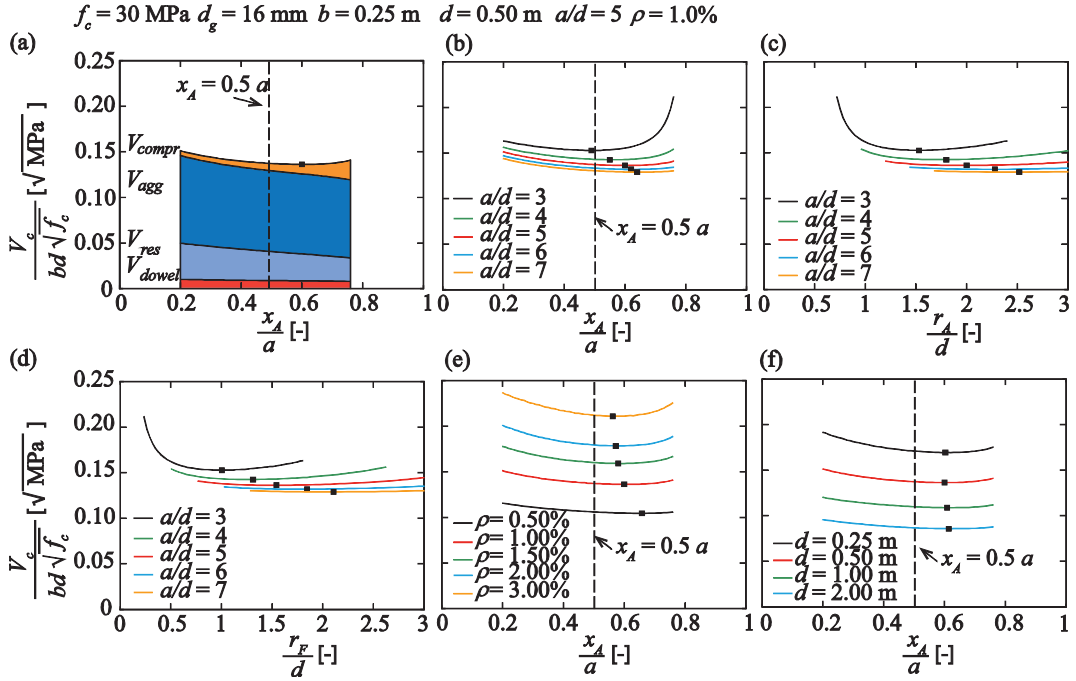


**Fig. 10.** Normalized shear strength as a function of the location of the critical crack (points in black refer to the location with the minimum shear strength): (a) contribution of the different shear-transfer actions at different critical crack locations $x_A$; (b–d) influence on the location of the critical shear crack of the slenderness ratio $a/d$, (e) of the longitudinal reinforcement ratio ρ and (f) of the effective depth $d$.

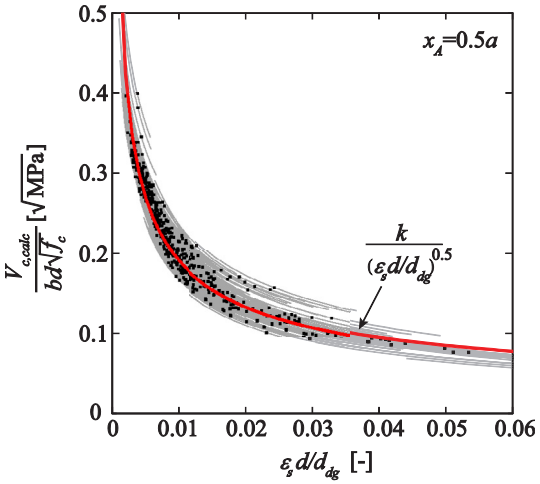


**Fig. 11.** Calculated shear strengths of 635 rectangular beams failing in shear ($a/d \geq 2.5$) (data from Reineck et al. [31] completed with the tests by Cavagnis et al. [11]) as a function of the reinforcement strains at the critical section ($x_A = 0.5a$).

0–32 mm, shear span $a$ ranging $2.5d - 8.5d$).

For design purposes, instead of calculating the failure criteria by integration of the stresses along the critical shear crack, Muttoni et al. [3] proposed a simple hyperbolic failure criterion (Fig. 1g) that approximates the failure band. Although the CSCT failure criterion provides a reasonable estimate of the shear capacity, Fig. 11 shows that its accuracy can be enhanced for low values of the term $\varepsilon_s \cdot d/d_{dg}$ with a power low expression (red line in Fig. 11) where the exponent of the term $\varepsilon_s \cdot d/d_{dg}$ is $-1/2$:

$$v_c = \frac{V_c}{b} = \frac{k \cdot d \cdot \sqrt{f_c}}{\sqrt{\varepsilon_s \cdot d/d_{dg}}} \leqslant v_{c0} \quad (34)$$

where $v_c$ is the shear capacity per unit length, $k$ is a constant that can be obtained by fitting of the calculated shear strengths ($k = 0.019$ in Fig. 11) and $v_{c0}$ refers to the maximum shear strength per unit length (not investigated in this study).

## 6. Validation of the approach with test results and improvement of the CSCT

Fig. 12 shows the comparison between the shear strengths calculated according to the general procedure (Eq. (5) + Eq. (33)), the simplified approach (Eq. (3) + Eq. (34)) and the original procedure of the CSCT [3] with some selected experimental test series. The main parameters governing the shear strength are investigated: the shear-to-span ratio $a/d$, the longitudinal reinforcement ratio ρ, the effective depth $d$, the compressive strength $f_c$, the aggregate size $d_g$ and the elastic modulus of the longitudinal bars $E_s$. The comparison shows that the calculated shear strengths are in very good agreement when compared with experimental results and the three approaches follow similar trends.

Fig. 13 presents a systematic comparison of the shear strengths calculated solving the set of Eqs. (5) and (33) against 635 tests on simply supported beams or cantilevers subjected to point loading (see also Appendix B). The database used is that of Reineck et al. [31] completed with the tests by Cavagnis et al. [11], where only rectangular beams with $a/d \geq 2.5$ have been considered. It can be observed that there are no clear trends for the main mechanical and geometrical parameters. The average measured-to-calculated shear strength is 1.01 and the Coefficient of Variation is 13.6% (Appendix B and Table 1).

The accuracy of the model is comparable to that obtained using the original formulation of the CSCT [3] (average measured-to-calculated shear strength 1.02, CoV 15.6%, refer to Table 1). Based on the observations of the present study and recent experimental investigations [24], the CSCT [3] can be improved accounting for $d_{dg}$ defined according to Eq. (17) (the ratio between measured-to-calculated shear

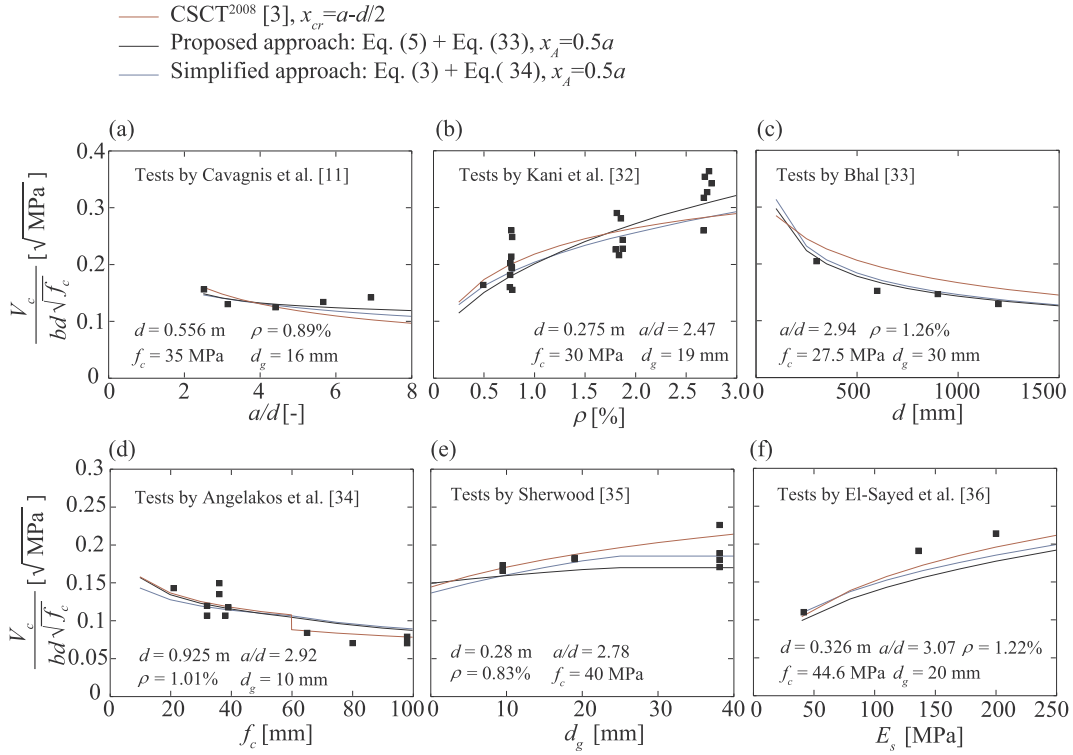


**Fig. 12.** Comparison of the refined proposed approach (black lines). the simplified approach (light blue lines) and the CSCT [3] (red lines) to test series investigating: (a) the slenderness ratio $a/d$ [11], (b) the reinforcement ratio ρ [32], (c) the effective depth $d$ [33], (d) the compressive strength $f_c$ [34], (e) the aggregate size $d_g$ [35] and (f) the reinforcement elastic modulus $E_s$ (steel and non-metallic reinforcements) [36]. (For interpretation of the references to colour in this figure legend, the reader is referred to the web version of this article.)

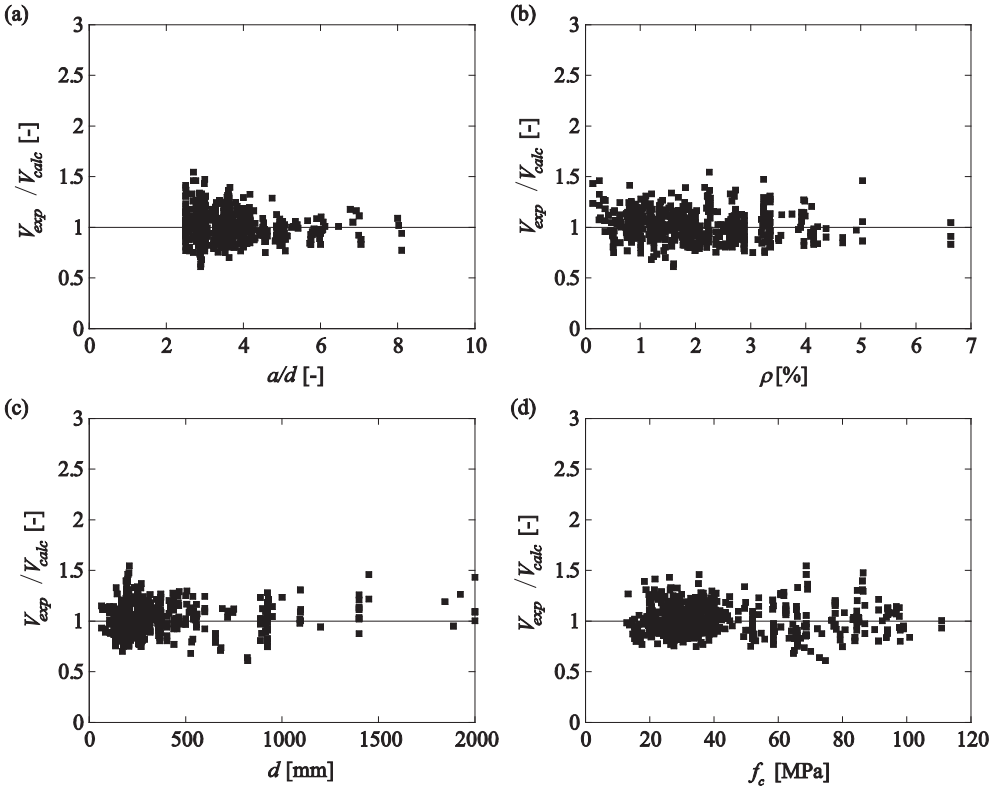


**Fig. 13.** Ratio $V_{exp}/V_{calc}$ ($V_{calc}$ calculated according to the presented procedure: Eqs. (5) and (33), assuming $x_A = 0.5a$) as a function of the different mechanical and geometrical parameters for the cases of slender simply supported beams and cantilevers subjected to concentrated load (data from Reineck et al. [31] completed with the tests by Cavagnis et al. [11]): (a) shear span-to-effective depth ratio $a/d$; (b) longitudinal reinforcement ratio ρ; (c) effective depth $d$ and (d) compressive strength $f_c$.

strength results equal to 1.01 with a CoV of 14.5%, refer to Table 1).

Moreover, as shown in Section 5, the accuracy of the hyperbolic failure criterion of the CSCT can be enhanced assuming a power law failure criterion (refer to Fig. 11). The shear capacity can thus be calculated in a simple manner by combining the load-deformation relationship of Eq. (3) and the simplified power law failure criterion of Eq. (34), assuming the control section at $x_A = 0.5a$. For this simplified approach, a good agreement is also found between the measured shear strength in the tests and the calculated one, with an average ratio of 1.03 and with a value of CoV of 14.2% (Table 1).

## 7. Conclusions

This paper presents an overview of the shear-transfer actions and their contribution to the shear strength of slender reinforced concrete members without transverse reinforcement. The contribution of the various shear-transfer actions is quantified on the basis of fundamental constitutive laws and accounting for a realistic crack shape and kinematics (based on detailed measurements on tests). The main conclusions are listed below:

(1) Shear can be carried by a number of potential shear transfer actions. In a general manner, there is not a governing shear transfer action, and the amount of shear force carried by each action depends on the location of the critical shear crack, its kinematics (opening and sliding) and the crack roughness properties.
(2) The cantilever action (as described in the Kani's tooth model) is governing for load levels which are generally lower than the actual failure load. This shear-carrying action is disabled by the development of a horizontal branch of the critical shear crack generated by the tensile stresses near the crack tip. The load can further be increased above the capacity of the cantilever action as other shear-carrying actions develop.
(3) For slender members, the failure load is eventually governed by beam shear-transfer actions (aggregate interlock, residual tensile strength, dowelling action and inclination of the compression chord):
   – For low crack widths in slender members, both aggregate interlock and tensile strength of concrete play an important role. For large crack widths, aggregate interlock becomes more dominant.
   – The dowelling action of the longitudinal reinforcement exhibits a more limited contribution than the other beam shear-carrying actions. Yet, its contribution is not necessarily negligible.
   – The contribution of the inclined compression chord for slender members depends significantly on the location of the tip of the critical shear crack. For critical shear cracks located at a certain distance from the load introduction, its contribution is rather low.

For squat members, arching action is governing.

**Table 1**
Comparison of calculated and experimental shear strengths: average value $V_{exp}/V_{calc}$ and coefficient of variation (CoV).

| | $V_{exp}/V_{calc}$ [−] | CoV [−] |
|---|---|---|
| CSCT$^{2008}$ [3], $x_{cr} = a\text{-}d/2$ | 1.02 | 0.156 |
| Proposed approach Eq. (5) + Eq. (33), assuming $x_A = 0.5a$ | 1.01 | 0.136 |
| Improvement of the CSCT$^{2008}$ [3] assuming $d_{dg}$ according to Eq. (17) | 1.01 | 0.145 |
| Simplified power law failure criterion Eq. (3) + Eq. (34), assuming $x_A = 0.5a$ | 1.03 | 0.142 |

(4) Despite the fact that the relative amount of each shear-transfer action may differ depending on the location and shape of the critical shear crack, the total shear capacity (sum of the various contributions) is relatively constant independently of the location of the critical shear crack. This explains why the location of the failure crack may vary significantly even for similar specimens.
(5) The force transferred by the different shear-transfer actions decay for increasing openings of the critical shear crack and they are governed by the same mechanical parameters. Accounting for this fact and for the relatively constant sum of the various shear-transfer actions, shear failures can be described by a single failure criterion.
(6) The main assumptions of the Critical Shear Crack Theory are in agreement to the previous conclusions and allow describing shear failures in a general manner. The shape of its failure criterion can be derived by analytical and numerical considerations, allowing relating the shear strength to the deformation capacity at failure, and it can be enhanced for low values of crack opening with a power law equation.

## Acknowledgement

The authors would like to gratefully acknowledge the support and funding of the Swiss Federal Road Authority, through the project AGB-2011-0.15.

## Appendix A: Notation

| | |
|---|---|
| $a$ | shear span (defined for specimens subjected to concentrated loads as the distance between the centre of the load and the centre of the support) |
| $a_A$ | $M/V$ at section A |
| $a_F$ | $M/V$ at section F |
| $b$ | width of the beam |
| $b_{ef}$ | effective width of concrete in tension |
| $c$ | depth of the compression zone |
| $c_1$, $c_2$, $c_3$, $c_4$ | constants of the model |
| $c_b$ | concrete cover |
| $c_m$ | distance from the top compression fibre to the centre of the inclined compression strut at the edge of the loading plate |
| $c_n$ | distance from the top compression fibre to the axis where inclined force of the compression zone acts |
| $d$ | effective flexural depth |
| $d_b$ | diameter of reinforcing bar |
| $d_{dg}$ | $d_g + 16$ [mm] |
| $d_F$ | vertical position of the tip of the crack |
| $d_g$ | maximum aggregate size |
| $f_c$ | concrete compressive strength measured in cylinder |
| $f_{ct}$ | concrete tensile strength |
| $f_{ct,ef}$ | effective tensile strength of concrete |
| $h$ | beam height |
| $h_F$ | distance from the top compression fibre to the tip of the shear crack |
| $k$ | coefficient power-law failure criterion |
| $k_b$ | reduction factor tensile strength of concrete |
| $k_c$ | coefficient compression zone |
| $l$ | span length |
| $l_1$ $l_2$ $l_3$ $l_{F1}$ | integration limits |
| $l_{ef}$ | effective length |
| $l_A$ | length of segment A-B of the critical shear crack |
| $l_B$ | length of the region of the beam contributing to the opening of the critical crack |
| $l_F$ | length of segment B-F of the critical shear crack |
| $n$ | number of longitudinal bars |
| $r_A$ | horizontal distance from the axis of the load introduction to the onset of the critical shear crack |
| $r_F$ | horizontal distance from the axis of the load introduction to the tip of the critical shear crack |
| $r_{F,edge}$ | horizontal distance from the edge of the loading plate to the tip of the critical shear crack |
| $u$ | opening of the crack measured along the horizontal direction |
| $u_A$ | horizontal opening of the critical shear crack at point A |
| $v$ | opening of the crack measured along the vertical direction |
| $v_A$ | vertical opening of the critical shear crack at point A |
| $v_c$ | shear capacity per unit length |
| $v_{c0}$ | maximum shear strength per unit length |
| $w$ | crack width perpendicular to the crack surface |
| $\overline{w}$ | normalized crack opening $w/d_{dg}$ |
| $w_A$ | opening perpendicular to the crack surface at point A |
| $w_B$ | opening perpendicular to the crack surface at point B along segment A-B |
| $w_c$ | maximum crack width allowing tensile stresses to develop in cracked concrete |
| $x_A$ | horizontal distance from the support to point A |
| $x_F$ | horizontal distance from the support to point F |
| $z$ | inner level arm |
| $A_s$ | area of longitudinal bars |
| $E_c$ | modulus of elasticity of concrete |
| $E_s$ | modulus of elasticity of steel |

| | |
|---|---|
| $G_F$ | fracture energy |
| $M$ | bending moment |
| $M_F$ | bending moment at the section corresponding to the tip of the critical shear crack |
| $N_{Agg}$ | horizontal component of the aggregate interlock action |
| $N_{Compr}$ | horizontal component of the inclined compression chord |
| $N_{Res}$ | horizontal component of the residual tensile strength of concrete |
| $V$ | acting shear force |
| $V_c$ | shear capacity |
| $V_{max}$ | shear force at failure (maximum value) |
| $V_{Agg}$ | shear force carried by aggregate interlock action |
| $V_{Compr}$ | shear force carried by inclined compression chord |
| $V_{Dowel}$ | shear force carried by dowelling action |
| $V_{Res}$ | shear force carried by residual tensile strength of concrete |
| $\alpha_c$ | inclination of the compression chord |
| $\alpha_A$ | $M_A/(V_A \cdot d)$ in section A |
| $\beta_{AB}$ | angle of quasi-vertical segment of the critical shear crack (segment AB) |
| $\beta_{BF}$ | angle of quasi-horizontal segment of the critical shear crack (segment BF) |
| $\gamma$ | secant mixed mode angle |
| $\gamma_T$ | tangent mixed mode angle |
| $\delta$ | crack sliding |
| $\delta_A$ | crack sliding at point A |
| $\overline{\delta}$ | normalized crack sliding $\delta/d_{dg}$ |
| $\varepsilon_s$ | steel strain |
| $\eta$ | integration variable for the residual tensile stresses |
| $\xi$ | integration variable for the aggregate interlock stresses |
| $\rho$ | reinforcement ratio of tension reinforcement |
| $\sigma_{agg}$ | aggregate interlock normal stress |
| $\sigma_{res}$ | residual tensile stress |
| $\tau_{agg}$ | aggregate interlock shear stress |
| $\psi$ | rotation of the critical shear crack |

## Appendix B

Test series considered in this study and comparison with the proposed expressions: Eq. (5) + Eq. (33).

| Researchers | No. of specimens | $f_c$ [MPa] | $b$ [mm] | $d$ [mm] | $a/d$ [−] | ρ [%] | $V_{exp}/V_{calc}$ (COV) |
|---|---|---|---|---|---|---|---|
| Adebar et al. [37] | 5 | 49.3–58.9 | 290–360 | 178–278 | 2.92–4.56 | 0.99–3.04 | 0.84 (0.068) |
| Ahmad et al. [38] | 17 | 63.4–68.7 | 127 | 184–208 | 2.70–4.00 | 1.77–6.64 | 1.03 (0.210) |
| Ahmad et al. [39] | 3 | 43.6–80.8 | 102 | 178 | 3.70 | 1.40 | 0.95 (0.070) |
| Angelakos et al. [34] | 7 | 21–80 | 300 | 895–925 | 2.88–2.97 | 0.50–2.09 | 0.96 (0.146) |
| Aster et al. [40] | 5 | 24.6–30.4 | 1000 | 250–750 | 3.65–3.68 | 0.42–0.91 | 1.01 (0.072) |
| Lubell et al. [41] | 11 | 37.1–64.6 | 250–3005 | 306–916 | 2.87–3.27 | 0.76–0.93 | 1.12 (0.089) |
| Bernander [42] | 6 | 27.6–29.1 | 100 | 168 | 4.17 | 0.97–1.17 | 1.07 (0.062) |
| Bhal [33] | 8 | 23.2–29.6 | 240 | 300–1200 | 2.94 | 0.63–1.26 | 1.03 (0.114) |
| Bresler et al. [43] | 3 | 22.6–37.6 | 305–310 | 461–466 | 3.80–6.77 | 1.81–2.73 | 1.24 (0.046) |
| Cladera et al. [44] | 6 | 49.9–87 | 200 | 360 | 2.90 | 2.23 | 1.00 (0.135) |
| Cao [45] | 2 | 27.5–30.1 | 300 | 1845–1925 | 2.77–2.89 | 0.36–1.52 | 1.23 (0.042) |
| Cederwall et al. [46] | 1 | 29.3 | 135 | 234 | 3.42 | 1.07 | 1.24 (−) |
| Chana [47] | 23 | 20.8–38.9 | 60–203 | 106–356 | 3.00 | 1.74–1.78 | 1.02 (0.073) |
| Chang et al. [48] | 15 | 17.7–38.6 | 102 | 137 | 2.60–4.09 | 1.86–2.89 | 0.91 (0.115) |
| Collins et al. [25] | 7 | 36–98 | 300 | 925 | 2.88 | 1.01 | 1.07 (0.156) |
| Diaz de Cossio et al. [49] | 5 | 19.5–31.5 | 152 | 254 | 3.30–5.30 | 0.98–3.33 | 0.99 (0.061) |
| Thorenfeldt et al. [50] | 14 | 54–97.7 | 150–300 | 207–442 | 3.00–4.00 | 1.82–3.24 | 1.15 (0.119) |
| Elzanaty et al. [51] | 11 | 20.7–79.3 | 177.8 | 267–273 | 4.00–6.00 | 0.93–3.21 | 0.88 (0.060) |
| Feldman et al. [52] | 8 | 21.5–36.7 | 152 | 252 | 2.87–6.04 | 3.35 | 1.11 (0.141) |
| Ferguson [53] | 1 | 29.3 | 101 | 189 | 3.23 | 2.08 | 0.82 (−) |
| Ghannoum [54] | 22 | 34.2–58.6 | 400 | 65–889 | 2.50 | 1.15–2.00 | 0.98 (0.110) |
| Grimm [55] | 11 | 90.1–110.9 | 300 | 146–746 | 3.53–3.90 | 0.83–4.22 | 1.00 (0.130) |
| Hallgreen [56] | 23 | 31.1–92.4 | 150–337 | 191–211 | 2.61–3.66 | 0.57–4.11 | 1.21 (0.084) |
| Hamadi [57] | 4 | 21.0–30.4 | 100 | 370–372 | 3.37–5.90 | 1.08–1.79 | 1.17 (0.082) |
| Hanson [58] | 4 | 20.9–31.0 | 152 | 267 | 4.95 | 1.25–3.50 | 0.97 (0.073) |
| Hedman et al. [59] | 4 | 19.9–29.5 | 152 | 267 | 4.95 | 1.25–2.22 | 1.03 (0.051) |
| Islam et al. [60] | 5 | 26.6–83.3 | 150 | 203–207 | 3.86–3.94 | 2.03–3.22 | 1.02 (0.105) |
| Johnson et al. [61] | 1 | 55.9 | 305 | 539 | 3.10 | 2.49 | 0.82 (−) |

| | | | | | | | |
|---|---|---|---|---|---|---|---|
| Kani [62] | 37 | 24.8–30.8 | 150–612 | 132–1097 | 2.50–8.03 | 2.59–2.87 | 1.02 (0.106) |
| Kani et al. [32] | 52 | 15.4–36.7 | 149–157 | 264–287 | 2.50–5.97 | 0.49–2.83 | 0.95 (0.108) |
| Kawano et al. [63] | 8 | 20.6–27.3 | 105–600 | 300–2000 | 3.00 | 1.18–1.37 | 1.06 (0.099) |
| Kim et al. [64] | 18 | 52 | 170–300 | 142–915 | 3.00–6.00 | 1.01–4.68 | 0.94 (0.087) |
| Krefeld et al. [65] | 50 | 12.9–39.0 | 152–254 | 238–483 | 2.67–8.10 | 0.80–4.92 | 0.95 (0.092) |
| Küng [66] | 7 | 18.4–21.7 | 140 | 200 | 2.50 | 0.36–1.82 | 1.20 (0.154) |
| Kuhlmann et al. [67] | 2 | 49.6 | 402 | 250 | 2.86–4.86 | 1.56 | 1.23 (0.121) |
| Kuhlmann et al. [68] | 4 | 43.4–47.6 | 400 | 250 | 2.86–4.86 | 1.57–1.92 | 1.05 (0.033) |
| Kulkarni et al. [69] | 4 | 40.6–43.6 | 102 | 152 | 3.50–5.00 | 1.38 | 1.04 (0.053) |
| Laupa et al. [70] | 6 | 14.8–32.3 | 152 | 262–269 | 4.82–4.95 | 1.91–3.97 | 0.89 (0.062) |
| Leonhardt et al. [30] | 26 | 13.3–38.3 | 50–500 | 70–600 | 2.78–5.91 | 1.33–2.40 | 1.01 (0.113) |
| Marti et al. [71] | 2 | 29.3–29.5 | 400 | 167 | 3.83 | 1.38–1.84 | 1.18 (0.029) |
| Mathey et al. [72] | 9 | 23.5–30.6 | 203 | 403 | 2.84–3.78 | 0.47–2.54 | 0.93 (0.085) |
| Moody et al. [73] | 23 | 15.4–41.2 | 152–178 | 262–272 | 2.85–3.41 | 1.60–2.37 | 0.95 (0.078) |
| Morrow et al. [74] | 12 | 14.7–45.7 | 305–308 | 356–375 | 3.00–8.10 | 1.27–3.91 | 1.00 (0.045) |
| Mphonde et al. [75] | 9 | 21.3–96.1 | 152.4 | 298 | 3.49 | 2.33–3.34 | 1.07 (0.043) |
| Niwa et al. [76] | 3 | 24.6–27.1 | 300–600 | 1000–2000 | 2.98 | 0.14–0.28 | 1.25 (0.135) |
| Podgomiak [77] | 8 | 37–99 | 300 | 225–925 | 2.88–2.97 | 0.51–3.14 | 0.98 (0.101) |
| Rajagopalan et al. [78] | 10 | 23.7–36.6 | 151–154 | 259–268 | 3.83–4.27 | 0.25–1.73 | 0.99 (0.170) |
| Regan [79] | 5 | 24.5–29.9 | 152 | 272 | 3.27 | 1.46 | 1.06 (0.076) |
| Rehm et al. [80] | 1 | 23.7 | 900 | 313 | 3.19 | 1.21 | 1.18 (−) |
| Reineck et al. [81] | 3 | 24.6–25.8 | 500 | 225–226 | 2.50–3.50 | 0.79–1.39 | 1.02 (0.032) |
| Remmel [82] | 4 | 84.5–85.1 | 150 | 160–165 | 3.06–4.00 | 1.87–4.09 | 0.97 (0.053) |
| Rüsch et al. [83] | 3 | 23–24.2 | 90–180 | 111–262 | 3.60 zo 3.62 | 2.64–2.65 | 0.87 (0.014) |
| Salandra et al. [84] | 4 | 53–70.1 | 102 | 171 | 2.59–3.63 | 1.45 | 0.83 (0.127) |
| Scholz [85] | 7 | 80.6–96.8 | 200 | 362–372 | 3.00–4.00 | 0.81–3.36 | 1.01 (0.132) |
| Taylor [86] | 6 | 27.8–33.2 | 203 | 370 | 3.02–3.50 | 1.03–1.55 | 1.09 (0.104) |
| Taylor [87] | 5 | 22–28.7 | 200–400 | 465–930 | 3.01 | 1.35 | 1.12 (0.090) |
| Walraven [88] | 3 | 24.1–24.4 | 200 | 125–720 | 3.00 | 0.74–0.83 | 1.07 (0.077) |
| Xie et al. [89] | 2 | 38.5–100.9 | 127 | 216 | 2.93 | 2.08 | 0.83 (0.022) |
| Yoon et al. [90] | 3 | 36–87 | 375 | 655 | 3.23 | 2.88 | 0.83 (0.052) |
| Yoshida [91] | 1 | 33.6 | 300 | 1890 | 2.82 | 0.74 | 0.95 (−) |
| Lubell [92] | 7 | 36.9–41 | 249–1170 | 287–538 | 2.91–3.57 | 0.33–1.73 | 1.19 (0.079) |
| Sherwood [35] | 21 | 28.1–77.3 | 122–300 | 280–1450 | 2.77–2.87 | 0.25–0.83 | 1.11 (0.111) |
| Thiele [93] | 5 | 24.6–42.5 | 400 | 167–297 | 3.47–4.97 | 0.93–2.41 | 1.05 (0.092) |
| Winkler [94] | 5 | 35.1 | 150–450 | 200–900 | 3.91–3.94 | 1.18–1.20 | 1.09 (0.067) |
| Rosenbusch [95] | 2 | 43.4 | 200 | 260 | 3.37 | 0.65–3.55 | 0.98 (0.077) |
| Tureyen et al. [96] | 3 | 40.9–43.7 | 457 | 360 | 3.38 | 0.36–1.92 | 1.07 (0.121) |
| Bentz et al. [97] | 9 | 34.3–36.1 | 101–106 | 84–333 | 2.80–2.94 | 1.55–1.63 | 1.05 (0.091) |
| Sneed et al. [98] | 8 | 64.8–74.8 | 203–613 | 233–822 | 2.87–2.92 | 1.20–1.60 | 0.79 (0.290) |
| Cavagnis et al. [11] | 6 | 32.6–35.6 | 250 | 556–559 | 2.52–6.92 | 0.54–0.89 | 1.04 (0.078) |
| | 635 | | | | | | **1.01 (0.136)** |

## Appendix C. Supplementary material

Supplementary data associated with this article can be found, in the online version, at http://dx.doi.org/10.1016/j.engstruct.2017.12.004.

## References


[1] Collins MP, Mitchell D, Adebar P, Vecchio F. A general shear design method. ACI Struct J 1996;93:36–45.
[2] Park H-G, Choi K-K, Wight JK. Strain-based shear strength model for slender beams without web reinforcement. ACI Struct J 2006;103:783–93.
[3] Muttoni A, Fernández Ruiz M. Shear strength of members without transverse reinforcement as function of critical shear crack width. ACI Struct J 2008;105:163–72.
[4] Yang Y, Walraven J, den Uijl J. Shear behavior of reinforced concrete beams without transverse reinforcement based on critical shear displacement. J Struct Eng 2016;143:4016146.
[5] Tung ND, Tue NV. A new approach to shear design of slender reinforced concrete members without transverse reinforcement. Eng Struct 2016;107:180–94.
[6] Fisker J, Hagsten LG. Mechanical model for the shear capacity of R/C beams without stirrups: A proposal based on limit analysis. Eng Struct 2016;115:220–31.
[7] Marí A, Bairán J, Cladera A, Oller E, Ribas C. Shear-flexural strength mechanical model for the design and assessment of reinforced concrete beams. Struct Infrastructure Eng: Maintenance, Manage, Life-Cycle Des Perform 2014;8:337–53.
[8] Fernández Ruiz M, Muttoni A, Sagaseta J. Shear strength of concrete members without transverse reinforcement: a mechanical approach to consistently account for size and strain effects. Eng Struct 2015;99:360–72.
[9] Campana S, Anastasi A, Fernández Ruiz M, Muttoni A. Analysis of shear-transfer actions on one-way RC members based on measured cracking pattern and failure kinematics. Mag Concr Res 2013;65:386–404.
[10] Cavagnis F, Fernández Ruiz M, Muttoni A. Shear failures in reinforced concrete members without transverse reinforcement: An analysis of the critical shear crack development on the basis of test results. Eng Struct 2015;103:157–73.
[11] Cavagnis F, Fernández Ruiz M, Muttoni A. An analysis of the shear transfer actions in reinforced concrete members without transverse reinforcement. Struct Conc 2017. http://dx.doi.org/10.1002/suco.201700145.
[12] Huber P, Huber T, Kollegger J. Investigation of the shear behavior of RC beams on the basis of measured crack kinematics. Eng Struct 2016;113:41–58.
[13] Reineck K-H. Ultimate shear force of structual concrete members without transverse reinforcement derived from a mchanical model. ACI Struct J 1991;88:592–602.
[14] Zararis PD, Papadakis GC. Diagonal shear failure and size effect in RC beams without web reinforcement. J Struct Eng 2001;127:733–42.
[15] Reinhardt HW. Fracture mechanics of an elastic softening material like concrete. Heron 1984;29:42.
[16] Fédération Internationale du Béton (fib), fib Model Code for Concrete Structures 2010, Ernst & Sohn 2013:434.
[17] CEB-FIP Model Code. Design code. London: Thomas Telford; 1990. p. 1993.
[18] Walraven JC. Fundamental analysis of aggregate interlock. J Struct Div 1981;107:2245–70.

[19] Gambarova PG, Karakoc C. A new approach to the analysis of the confinement role in regularly cracked concrete elements. In: Transactions of the 7 international conference on structural mechanics in reactor technology 1983; H.
[20] Li B. Contact density model for stress transfer across cracks in concrete. J Faculty Eng, the Univ Tokyo 1989;1:9–52.
[21] Ulaga T. Betonbauteile mit Stab- und Lamellenbewehrung: Verbund- und Zuggliedmodellierung. PhD Thesis. Thesis no. 15062 (in German). Zurich, Switzerland: ETHZ; 2003:160.
[22] Guidotti R. Poinçonnement des planchers-dalles avec colonnes superposées fortement sollicitées. PhD Thesis. Thesis no. 4812 (in French). Lausanne, Switzerland: Ecole Polytechnique Fédérale de Lausanne; 2010:416.
[23] Jacobsen JS, Poulsen PN, Olesen JF. Characterization of mixed mode crack opening in concrete. Mater Struct 2012;45:107–22.
[24] Sherwood EG, Bentz EC, Collins MP. Effect of aggregate size on beam-shear strength of thick slabs. ACI Struct J 2007;104:180–90.
[25] Collins MP, Kuchma D. How safe are our large, lightly reinforced concrete beams, slabs, and footings? ACI Struct J 1999;96:482–90.
[26] Fernández Ruiz M, Mirzaei Y, Muttoni A. Post-punching behavior of flat slabs. ACI Struct J 2013;110:801–12.
[27] Fernández Ruiz M, Plumey S, Muttoni A. Interaction between bond and deviation forces in spalling failures of arch-shaped members without transverse reinforcement. ACI Struct J 2010;107:346–54.
[28] Fernández Ruiz M, Campana S, Muttoni A. Discussion of paper “Influence of Flexural Reinforcement on Shear Strength of Prestressed Concrete Beams” by E. I. Saquan and R.J. Frosch. ACI Struct J 2009;106:907–8.
[29] Calvi PM, Bentz EC, Collins MP. Reversed cyclic experiments on shear stress transfer across cracks in reinforced concrete elements. ACI Struct J 2016;113:851–9.
[30] Leonhardt F, Walther R. Schubversuche an einfeldrigen Stahlbetonbalken mit und ohne Schubbewehrung. DAfStb H.151, Berlin 1962.
[31] Reineck K, Bentz EC, Fitik B, Kuchma DA, Bayrak O. ACI-DAfStb database of shear tests on slender reinforced concrete beams without stirrups. ACI Struct J 2013;110:867–76.
[32] Kani MW, Huggins MW, Wittkopp RR. Kani on shear in reinforced concrete. Toronto, Canada: Deptartment of Civil Engineering, University of Toronto; 1979.
[33] Bhal NS. Über den Einfluß der Balkenhöhe auf die Schubtragfähigkeit von einfeldrigen Stahlbetonbalken mit und ohne Schubbewehrung. Otto-Graf-Institut, H.35, Stuttgart, Germany; 1968.
[34] Angelakos D, Bentz EC, Collins MP. Effect of concrete strength and minimum stirrups on shear strength of large members. ACI Struct J 2001;98:290–300.
[35] Sherwood EG. One-way shear behaviour of large, lightly-reinforced concrete beams and slabs. PhD Thesis, Toronto, Canada: University of Toronto; 2008. p. 547.
[36] El-Sayed AK, El-Salakawy EF, Benmokrane B. Shear strength of FRP-reinforced concrete beams without transverse reinforcement. ACI Struct J 2006;103:235–43.
[37] Adebar P, Collins MP. Shear strength of members without transverse reinforcement. Can J Civ Eng 1996;23:30–41.
[38] Ahmad SH, Khaloo AR, Poveda A. Shear capacity of reinforced high-strength concrete beams. ACI Struct J 1986;83:297–305.
[39] Ahmad SH, Park F, El-Dash K. Web reinforcement effects on shear capacity of reinforced highstrength concrete beams. Mag Concr Res 1995;47:227–33.
[40] Aster H, Koch R. Schubtragfähigkeit dicker Stahlbetonplatten. Beton- Und Stahlbetonbau 1974;69:266–70.
[41] Lubell A, Sherwood T, Bentz E, Collins M. Safe shear design of large wide beams. Concr Int 2004;26:62–78.
[42] Bernander KG. An investigation of the shear strength of concrete beams without stirrups or diagonal bars, reinforced with high tensile steel with various rib patterns. In: Proc., RILEM symposium on bond and crack formation in reinforced concrete; 1957. p. 211–4.
[43] Bresler B, Scordelis AC. Shear strength of reinforced concrete beams. ACI J 1963;60:51–74.
[44] Cladera A, Marí A. Experimental study on high-strength concrete beams failing in shear. Eng Struct 2005;27:1519–27.
[45] Cao S. Size effect and the influence of longitudinal reinforcement on the shear response of large reinforcement concrete members. PhD Thesis, Toronto, Canada: Univerisity of Toronto; 2001.
[46] Cederwall K, Hedman O, Losberg A. Shear strength of partially prestressed beams with pretensioned reinforcement of high grade deformed bars. Special Publ 1974;42:215–30.
[47] Chana PS. Some aspects of modelling the behaviour of reinforced concrete under shear loading, Technical Report 43. Cement and Concrete Association; 1981. p. 22.
[48] Chang TS, Kesler CE. Static and fatigue strength in shear of beams with tensile reinforcement. ACI J 1958;54:1033–57.
[49] Diaz de Cossio R, Siess CP. Behavior and strength in shear of beams and frames without web reinforcement. ACI J 1960;31:695–735.
[50] Thorenfeldt E, Drangsholt G. Shear capacity of reinforced high-strength concrete beams. ACI Spec Publ 1990;121:129–54.
[51] Elzanaty AH, Nilson A, Slate FO. Shear capacity of reinforced concrete beams using high-strength concrete. ACI J 1986;83:290–6.
[52] Feldman A, Siess CP. Effect of moment shear ratio on diagonal tension cracking and strength in shear of reinforced concrete beams. Univ. of Illinois Civil Eng. Studies, Struct. Research Series No. 107 1955.
[53] Ferguson PM. Some implications of recent diagonal tension tests. ACI J Proc 1956;53:157–72.
[54] Ghannoum WM. Size effect on shear strength of reinforced concrete beams. McGill University Montréal, Canada: Department of Civil Engineering and Applied Mechanics; 1995.
[55] Grimm R. Einfluß bruchmechanischer Kenngrößen auf das Biege-und Schubtragverhalten hochfester Betone. Deutscher Ausschuss Fuer Stahlbeton; 1997. p. 477.
[56] Hallgren M. Shear tests on reinforced high and normal strength concrete beams without stirrups. Royal Institute of Technology, Stockholm, Sweden: Dept. of Structural Engineering; 1994.
[57] Hamadi YD. Force transfer across cracks in concrete structures, PhD Thesis, London, UK: Polytechnic of Central London; 1976.
[58] Hanson JA. Tensile strength and diagonal tension resistance of structural lightweight concrete. ACI J 1961;58:1–40.
[59] Hedman O, Losberg A. Design of concrete structures with regard to shear forces. CEB Bulletin D’Information No. 126; 1978.
[60] Islam MS, Pam HJ, Kwan AKH. Shear capacity of high-strength concrete beams with their point of inflection within the shear span. Proc Inst Civ Eng Struct Build 1998;128:91–9.
[61] Johnson MK, Ramirez JA. Minimum shear reinforcement in beams with higher strength concrete. ACI Struct J 1989;86:376–82.
[62] Kani GNJ. How safe are our large reinforced concrete beams? ACI J 1967;64:128–41.
[63] Kawano H, Watanabe H. Shear strength of reinforced concrete columns – Effect of specimen size and load reversal. Proceedings of the Second Italy-Japan Workshop on Seismic Design and Retrofit of Bridges 1997:141–54.
[64] Kim J-K, Park Y-D. Shear strength of reinforced high strength concrete beam without web reinforcement. Mag Concr Res 1994;46:7–16.
[65] Krefeld WJ, Thurston CW. Studies of the shear and diagonal tension strength of simply supported R/C-beams. ACI J 1966;63:451–76.
[66] Küng R. Ein Beitrag zur Schubsicherung im Stahlbetonbau. Betonstahl in Entwicklung, H.33. Luxemburg: TOR-ISTEG Steel Corp; 1985. p. 8–25.
[67] Kuhlmann U, Ehmann J. Versuche zur Ermittlung der Querkrafttragfähigkeit von Verbundplatten unter Längszug ohne Schubbewehrung. Versuchsbericht 2001-6X: Mitteilung; 2001.
[68] Kuhlmann U, Zilch K, Ehmann J, Jähring A, Spitra F. Querkraftabtragung in Verbundträgern mit schlaff bewehrter und aus Zugbeanspruchung gerissener Stahlbetonplatte ohne Schubbewehrung- Mitteilungen. Institut für Konstruktion und Entwurf Stahl-, Holz-, und Verbundbau, Universität Stuttgart, Germany; 2002. p. 109.
[69] Kulkarni SM, Shah SP. Response of reinforced concrete beams at high strain rates. ACI Struct J 1998;95:705–14.
[70] Laupa A, Siess CP, Newmark NM. The shear strength of simple-span reinforced concrete beams without web reinforcement. Research Series No. 52, University of Illinois at Urbana-Champaign, USA; 1953.
[71] Marti P, Pralong J, Thürlimann B. Schubversuche an Stahlbeton-Platten. IBK-Bericht No. 7305–2, ETH Zürich, Zürich, Switzerland; 1977.
[72] Mathey RG, Watstein D. Shear strength of beams without web reinforcement containing deformed bars of different yield strengths. ACI J 1963;60:183–207.
[73] Moody KG, Viest IM, Elstner RC, Hognestad E. Shear strength of R.C. beams: Part 1 – tests of simple beams. ACI J 1954;26:317–32.
[74] Morrow J, Viest IM. Shear strength of reinforced concrete frame members without web reinforcement. ACI J 1957;53:833–69.
[75] Mphonde AG, Frantz GC. Shear tests of high- and low- strength concrete beams without stirrups. ACI J 1984;81:350–7.
[76] Niwa J, Yamada K, Yokozawa K, Okamura M. Revaluation of the equation for shear strength of R.C.-beams without web reinforcement. Proceedings JSCE No. 372/V-5 1986–8 Translation. In: Concrete Library of JSCE, No. 9; 1987.
[77] Podgorniak-Stanik BA. He influence of concrete strength, distribution of longitudinal reinforcement, amount of transverse reinforcement and member size on shear strength of reinforced concrete members. PhD Thesis, Toronto, Canada: University of Toronto; 1998.
[78] Rajagopalan KS, Ferguson PM. Exploratory shear tests emphasizing percentage of longitudinal reinforcement. ACI J 1968;65:634–8.
[79] Regan PE. Shear in reinforced concrete – an experimental study. CIRIA-report, a report to the construction research and information association. Imperial College of Science and Technology, Dep. of Civil Engineering, Concrete Section; 1971.
[80] Rehm G, Eligehausen R, Neubert B. Rationalisierung der Bewehrungstechnik im Stahlbetonbau. Betonwerk + Fertigteil-Technik 1978;222–7.
[81] Reineck K-H, Koch R, Schlaich J. Shear tests on reinforced concrete beams with axial compression for offshore structures. Stuttgart, Germany: Institut für Massivbau, Universität Stuttgart; 1978.
[82] Remmel G. Zum Zugtragverhalten hochfester Betone und seinem Einfluß auf die Querkrafttragfähigkeit von schlanken Bauteilen ohne Schubbewehrung. PhD Thesis, Darmstadt, Germany: TH Darmstadt; 1991.
[83] Rüsch H, Haugli FR, Mayer H. Schubversuche an Stahlbeton Rechteckbalken mit Gleichmassig Verteilter Belastung, Deutscher Ausschuss fur Stahlbeton, Heft 145. West Berlin: W. Ernst und Sohn; 1962.
[84] Salandra MA, Ahmad SH. Shear capacity of reinforced lightweight high-strength concrete beams. ACI Struct J 1989;86:697–704.
[85] Scholz H. Ein Querkrafttragmodell für Bauteile ohne Schubbewehrung im Bruchzustand aus normalfestem und hochfestem Beton. Berichte aus dem Konstruktiven Ingenieurbau Heft 21, Technische Universität Berlin, Berlin, Germany; 1994.
[86] Taylor HPJ. Shear stress in reinforced concrete beams without shear reinforcement. Cement and Concrete Ass., Techn. Rep. No. 407; 1968.
[87] Taylor HPJ. Shear strength of large beams. ASCE J Struct Div 1972;98:2473–90.
[88] Walraven JC. The influence of depth on the shear strength of lightweight concrete beams without shear reinforcement. Report S-78-4, Stevin Lab., Delft University, Delft, Netherlands; 1978.
[89] Xie Y, Ahmad SH, Yu T, Hino S, Chung W. Shear ductility of reinforced concrete

beams of normal and high-strength concrete. ACI Struct J 1994;91:140–9.
[90] Yoon Y-S, Cook WD, Mitchell D. Minimum shear reinforcement in normal, medium and high- strength concrete beams. ACI Struct J 1996;93:576–84.
[91] Yoshida Y. Shear reinforcement for large lightly reinforced concrete members. PhD Thesis, Toronto, Canada: University of Toronto; 2000.
[92] Lubell A. Shear in wide reinforced concrete beams. PhD Thesis, Toronto, Canada: University of Toronto; 2006. p. 455.
[93] Thiele C. Zum Tragverhalten von Stahlbetonplatten ohne Querkraftbewehrung mit integrierten Leitungsführungen. PhD Thesis, Kaiserslautern, Germany: TU Kaiserslautern; 2010.
[94] Winkler K. Querkraftversuche an maßstäblich skalierten, schubunbewehrten Stahlbetonbalken. Versuchsbericht 2011–1. Lehrstuhl für Massivbau, Ruhr Universität Bochum, Bochum, Germany; 2011. p. 105.
[95] Rosenbusch J. Zur Querkrafttragfähigkeit von Balken aus stahlfaserverstärktem Stahlbeton. Germany: TU Braunschweig, Braunschweig; 2004.
[96] Tureyen AK, Frosch RJ. Shear tests of FRP-reinforced concrete beams without stirrups. ACI Struct J 2002;99:427–34.
[97] Bentz EC, Buckley S. Repeating a classic set of experiments on size effect in shear of members without stirrups. ACI Struct J 2005;102:832–8.
[98] Sneed LH, Ramirez JA. Influence of effective depth on shear strength of concrete beams - experimental study. ACI Struct J 2010;107:554–62.